ijlpr 2022; doi 10.22376/ijpbs/lpr.2022.12.1.L265-282

International Journal of Life science and Pharma Research

ISSN 2250-0480

Review Article

A Review On Electropsun Chitosan Fibers For Bone Tissue Defects

Nadeem Siddiqui [*1], Kotikalapudi Karthik[1], Monica Adapala[1], Vemparala Renuka[1], Goudu Yashwanth[1] And Siva Reddy Golamari[1]

[1]*Department of Biotechnology, Koneru Lakshmaiah Education Foundation, Guntur-Andhra Pradesh-India.*

[1]*Research Fellow, Biovalley Incubation council, Andhra Pradesh Med Tech Zone, Visakhapatnam, Andhra Pradesh-India.*

Abstract: Bone tissue engineering has been an evolving field for decades in view of its intrinsic potential to regenerate and the necessity of repair in response to injuries or disorders. Scaffold implantation is one of the most applied techniques to overcome the donor crisis leading to bone regeneration using osteoinducible cells. Numerous combinations of scaffold composites are being designed in-order to achieve the maximum regeneration considering the parameters such as bio-compatibility, biodegradability osteo conductivity, mechanical strength and hydrophilicity that helps in the assessment of the possible negative impacts of the healing process. This review article concentrates on some of such composites where the chitosan, a natural polymer, is combined with the other biopolymers like synthetic and ceramic polymers at various concentrations and treatments reporting the desired results. The distinct characteristic of this review is that it focuses on the scaffolds that are completely Nano fibrous in nature fabricated by electro spinning. In this review, we reported the results of various combinations of chitosan and their significance. The ability to form (Calcium and Phosphate crystals-Biomineralization) is evident that chitosan combined with the other biopolymers can be contemplated as phenomenal scaffold as the used seed cells are clinically applied across the world – human mesenchymal stem cells (hMSCs), bone marrow mesenchymal stem cells (BM-MSCs), mouse mesenchymal stem cells (mMSCs), human fetal osteoblasts (hFOB), etc. Apart from the *in-vitro* studies, the results of *in-vivo* experiments were also included in this article where the implantation targets the calvarial bone regeneration. Besides osteogenic differentiation, this article highlighted the prominent efficiency of the scaffolds to exhibit the antimicrobial activity and to act as drug delivery system when doped with components like $AgNO_3$, Chlorhexidine, ZnO and Amoxicillin, Sinapic acid respectively. Overall, in the current review, we tried to focus on consolidation of various results related to chitosan based nanofibers for bone tissue remodeling.

Keywords: Bone Regeneration, Osteo inducible cells, Chitosan, Nano Fibrous scaffold, Electrospinning, Osteo conductivity, antimicrobial activity, Drug Delivery System

***Corresponding Author**

Nadeem Siddiqui , Department of Biotechnology, Koneru Lakshmaiah Education Foundation, Guntur-Andhra Pradesh-India.

Received On 23 December, 2021
Revised On 18 January, 2022
Accepted On 27 January, 2022
Published On 28 January, 2022

Funding This research did not receive any specific grant from any funding agencies in the public, commercial or not for profit sectors.

Citation Nadeem Siddiqui, Kotikalapudi Karthik, Monica Adapala, Vemparala Renuka, Goudu Yashwanth And Siva Reddy Golamari , A Review On Electropsun Chitosan Fibers For Bone Tissue Defects.(2022).Int. J. Life Sci. Pharma Res.12(1), L265-282 http://dx.doi.org/10.22376/ijpbs/lpr.2022.12.1.L265-282

1. INTRODUCTION

Bone is a highly mineralized vascular tissue comprising 10% water, 30% matrix, 60% mineral[1]. It is an essential support structure safeguarding the internal organs of the body. Bone is a source of calcium and magnesium, which regulate acid-base balance, and blood cells are produced in the marrow cavity of the bone tissue [2]. There are two types of bone, namely the mechanically protective cortical bone and the metabolically active trabecular bone which aids in limb and joint movements [3,4]. The osteoblasts in the bone matrix produce new bone through a process called ossification by ligand-receptor interactions with the matrix. The primary processes for bone formation are intramembranous ossification and endochondral ossification. In intramembranous ossification, the new bone is formed directly by the primitive connective tissue. In endochondral ossification, the migrated mesenchymal stem cells (MSCs) first deposit a cartilaginous matrix that serves as a substrate for gradual replacement to bone tissue. The hydroxyapatite (HAP) inorganic component of the bone matrix, which is the crystalline form of pentacalcium hydroxide triphosphate, accounts for hardness and rigidity of bone. The organic component, composed of collagenous and non-collagenous proteins, provides elasticity, impact strength and fracture toughness to the bone. There are four cell types in the bone matrix, namely osteocytes, osteoclasts, osteoblasts, and bone lining cells. These cells dynamically regulate bone formation and resorption [5]. Bone defects that require a grafts or an implant to restore continuity are segmental, cavitary, discontinuity, and intercalary [6]. The graft is also called a bone scaffold if it involves tissue regeneration. The grafts or scaffolds are produced from composites of synthetic or natural polymers with ceramics [7]. Natural polymers, due to their biocompatibility and biodegradability, are used extensively as scaffolds or grafts for treating bone defects. Many approaches are used to produce porous scaffolds with different microstructure and morphology. Among them, electrospinning is widely used to produce nanofibers scaffolds that resemble the microstructure of extracellular collagenous matrix of the bone tissue [8]. Bone tissue engineering provides an alternative to autograft and allograft bone for treating bone defects by implantation of a natural or synthetic scaffold loaded with bone cells and morphogens to regenerate the injured osseous tissue [9]. Many techniques have been developed to produce porous scaffolds for tissue engineering applications [10]. Among them, the electrospinning technique is widely used to produce nanofibrous scaffolds for tissue engineering because the scaffold microstructure mimics that of the natural collagenous tissues. In electrospinning, the polymer solution is injected using a spinneret or needle into a chamber connected to a high-voltage electric field. Due to surface tension and electrostatic repulsion effects, the ejected droplets are stretched as nanofibers (NFs) in the electric field toward the collector [11]. The NFs are collected on the collector plate as a fibrous scaffold. Solution and process parameters affect the properties of the produced fibrous scaffold. Solution parameters include solvent type, polymer concentration, solution viscosity and conductivity [12] whereas process parameters consist of needle size, ejector-collector distance, intensity of the applied electric field [13]. Ambient conditions like temperature and humidity also affect the properties of the produced fibres. The intensity of the applied voltage is specific to the type of polymer and solvent used for electrospinning. A nanofibrous mesh is produced as the applied electric field is increased above a critical intensity. The fibre morphology is influenced by surface charge density of the droplets, needle-collector distance, solvent evaporation rate, instability interval of the spinning jet, fibre deposition time [14]. For solutions below a critical polymer concentration, the stretched droplets breakup by capillary action before reaching the collector and form beaded NFs [15]. The low conductivity of the electrospinning solution hinders the formation of a taylor cone and fibre formation due to low surface charge density of the spinning jet. Conversely, conductivity higher than a critical value promotes the formation of taylor cones and deposition of NFs with smaller average diameter [16]. The polymer should be miscible in the solvent. The boiling point of the solvent should be sufficiently low to allow evaporation during the time between injection in the electric field and deposition on the collector. Changes in ambient conditions like humidity can affect the drying and solidification of the spinning droplets and the final diameter of the generated fibres [17]. Temperature has two competing effects on the electrospinning process, namely solution viscosity and rate of solvent evaporation.

1.1 Properties And Processing Of Chitosan

Chitosan (CS) is a natural polysaccharide consisting of glucosamine and N- acetyl glucosamine units linked by 1,4 β-glycosidic bonds. Chitosan is the deacetylated form of chitin [18] and the purity of the produced chitosan depends on the degree of deacetylation and molecular weight of chitin. Chitosan is considered as the second most abundant animal-based biopolymer after collagen, which can be found in the skeletons of crustaceans, insects, and bacterial and fungal cell walls [19]. Chitosan is used in wound dressing, controlled drug release formulations as well as other medical and pharmaceutical applications [20]. The physico-chemical properties of chitosan can be tuned to a particular application , which makes this biomaterial a promising candidate for use as a scaffold in bone tissue engineering [21]. Further, chitosan has antioxidant, anti-microbial, and anti-tumor properties [22]. Chitosan can penetrate through the bacterial cell walls, integrate with DNA, and obstruct the process of translation of DNA codes into functional products [23]. Oxidative stress is a cause of numerous diseases including cancer and cardiovascular diseases [24,25]. Chitosan and its derivatives act as free-radical scavengers against highly stable hydroxyl, alkyl, and superoxide radicals as well as 2,2-diphenyl-1-picrylhydrazyl (DPPH) radicals . According to in vivo results, chitosan interferes with the growth of tumor cells by enhancing the immune response [26] which is attributed to the increased production of lymphokines that amplify the proliferation of cytotoxic T-lymphocytes [27]. The infiltration of cytotoxic T-lymphocytes and their maturation leads to an anti-tumor effect by the increased production of interleukin-1 (IL-1) and IL-2 [22]. Aside from its biocompatibility, non-allergenicity and biodegradability as key characteristics [28], chitosan possess antibacterial, anti-tumour, anti-fungal, immune-adjuvant, anti-thrombogenic, anti-cholesterol, and bio-adhesive activities [29]. Chitosan in the form of fibrous porous scaffolds is used in tissue regeneration of bone [30], cartilage [31], intervertebral disc [32], blood vessel [33], cornea [34] as well as wound regeneration [35]. Chitosan and its corresponding ionic complexes and their blends with synthetic or natural polymers are used in drug encapsulation, cell immobilization, and as a carrier in gene transfection [36].

The presence of polar groups that can have secondary interaction with other polymers as well as hydrophilicity, biodegradability, and anti-bacterial activity affords advantages to chitosan over other polymers for medical and pharmaceutical applications [37].

1.2 Chitosan Biocomposites

Chitosan, due to its biocompatibility and degradability, is studied extensively as a scaffold in tissue engineering [38]. Chitosan is blended with other natural polymers like collagen (COL), gelatin (GEL), alginate (ALG), hyaluronic acid (HLA) as well as synthetic polymers like poly(ε-polycaprolactone) (PCL), polylactide (PLA), poly(lactide-co-glycolide) (PLGA) and polyurethane (PU), and bio-ceramics such as HAP, tricalcium phosphate (TCP), Wollastonite and bio-glass to augment physical and biological properties [39]. In bone tissue engineering, mesenchymal stem cells (MSCs) or progenitor osteoblasts are seeded in a suitable scaffold and the construct is loaded with cell signalling molecules to guide the differentiation and maturation of cells to osteo-specific cell lineages for regeneration of the tissue after implantation [40].

1.3 Composites Of Chitosan With Natural Biopolymers

Aidun and collaborators investigated the effect of incorporation of Graphene oxide (GO) in electrospun Chitosan/PolycaproLactone /Collagen (CS/PCL/COL) composite scaffolds up to 6 wt% on morphology, hydrophilicity, biodegradation, swelling, bioactivity, cell compatibility, and the ability to support growth and differentiation of seeded cells [41]. The electrospinning parameters were injection rate of 0.6 mL/h, applied voltage of 20 kV and needle-collector distance of 12 cm. As the GO concentration was increased, diameter of the produced fibres decreased from 130 ± 30 nm to 115 ± 30 nm and contact angle decreased from 73° to 52°. The percentage swelling increased from 120±4% to 132±2% and bioactivity toward apatite deposition increased with increasing GO content. The incorporation of GO increased growth, adhesion, osteogenic differentiation, as measured by alkaline phosphatase activity, and mineralization as measured by Alizarin red staining, for human MG-63 osteosarcoma cells seeded on the electrospun fibrous scaffolds. However, GO incorporation did not have a noticeable effect on antibacterial activity and biodegradation of the fibres. Lai and co-workers produced composite fibrous membranes of CS with silk fibroin (SF) and nano-HAP (nHAP), hereafter referred to CS/SF/nHAP, by electrospinning employing a flow rate of 0.5 mL/h, voltage of 18 kV, and tip-collector distance of 12 cm [42]. The addition of nHAP to CS/SF membranes decreased the fibre diameter from 450±170 nm to 270±50 nm and tensile strength of the membranes was increased by 3-fold (0.38±0.11 MPa to 1.09±0.14MPa). Further, viability of MSCs was found to be higher on CS/SF/nHAP on day 14 compared to CS/SF membranes and alkaline phosphatase (ALP) activity of the cell-seeded membranes peaked on day 14, indicating that the membranes support osteogenic differentiation MSCs. The intensity of Alizarin red staining for mineralization by the seeded MSCs was higher on CS/SF/nHAP composite membranes as compared to CS/SF after 21 days of culture. The expression of osteopontin (OP) and osteocalcin (OC) by MSCs was higher on CS/SF/nHAP composites with 30 wt% nHAP as compared to those with 10 wt% and no nHAP. Chen and collaborators produced CS/GEL bilayer scaffolds reinforced with HAP by electrospinning [43]. The feed rate for CS and GL layers was 0.4 mL/h and 0.3 mL/h, respectively, with a voltage of 20 kV and tip-collector distance of 12 cm. The average fibre diameter in GL core and CS shell were 100 nm and 150 nm, respectively. Cell viability and growth, as measured by seeding human MG-63 osteosarcoma cells, improved by incorporating polyethylene oxide (PEO) in the scaffold (CS/PEO/GEL) as compared to Chitosan/Gelatin (CS/GEL) bilayer or GEL monolayer scaffolds, which was attributed to the higher hydrophilicity of PEO. Ghorbani et al. produced composite NFs of CS with nanocrystalline cellulose (nCC) by electrospinning using a feed rate of 2 mL/h, voltage of 15 kV and tip-collector distance of 10 cm [44]. The diameter and tensile strength of composite fibres were 259 nm and 19.1 MPa, respectively, compared to 299 nm and 7.6 MPa for pure CS fibres. Degradation of fibrous scaffolds decreased with increasing nCC content. The composite fibres had a contact angle in the range of 78-58° which was lower than that of pure CS at 83°, which was attributed to the higher hydrophilicity of crystalline cellulose. However, there was no noticeable difference in cell viability of 3T3 mouse embryonic fibroblasts seeded on composite CS/nCC or pure CS fibrous scaffolds. Ezzati et al. studied the effect of TCP incorporation on the properties of PCL/GEL/CS/β-TCP fibrous composites produced by electrospinning with flow rate of 0.9 mL/h, voltage of 10 kV, and tip-collector distance of 10 cm [45]. The average fibre diameter was 290 nm and fibre pore size decreased with the addition of β-TCP. The hydrophilicity of PCL/GEL/CS NFs increased with the addition of β-TCP because the water contact angle on the fibres decreased from 34.6 ± 0.6° to 25.5 ± 0.5° with 25.54 ± 0.48°. The surface roughness of the NFs increased from 52.6 ± 1.2 nm to 79.2 ± 1.4 nm with the addition of β-TCP, which would positively contribute to cell adhesion and cell-material interaction. The tensile strength of the NFs increased with the addition of β-TCP from 6 MPa to 7-9 MPa. The viability of MG-63 human osteosarcoma cells on PCL/GEL/CS NFs after 7 days of culture increased noticeably with the addition of 5 wt% β-TCP whereas cell proliferation was highest with 3 wt% β-TCP compared to other β-TCP loading in the range of 1-5 wt%. Jalala et al. synthesized CS/GEL core/shell NFs by electrospinning with GEL and CS as the core and shell, respectively, using a flow rate of 0.2 mL/h, applied potential of 25-30 kV, and tip-collector distance of 15 cm [46]. The synthesized fibres were further crosslinked using dextran aldehyde and sucrose to improve fibre stability in physiological medium. The average diameter of the synthesized fibres was 150±60 nm. The crosslinked CS/GEL fibres retained 45% of their mass after 5 weeks of incubation in simulated body fluid (SBF) whereas the un-cross linked fibres disintegrated in the same period. The tensile strength of the un-cross linked fibre mesh was 19 ± 3 MPa which increased to 65 ± 2 MPa upon crosslinking. The viability of MG-63 osteosarcoma cells on dextran aldehyde-sucrose crosslinked CS/GEL fibres cross linked fibre mesh was higher than the glutaraldehyde crosslinked fibres after 5 days of culture. Further, the cells on dextran aldehyde-sucrose crosslinked fibres had a well spread morphology as shown in Figure 1.

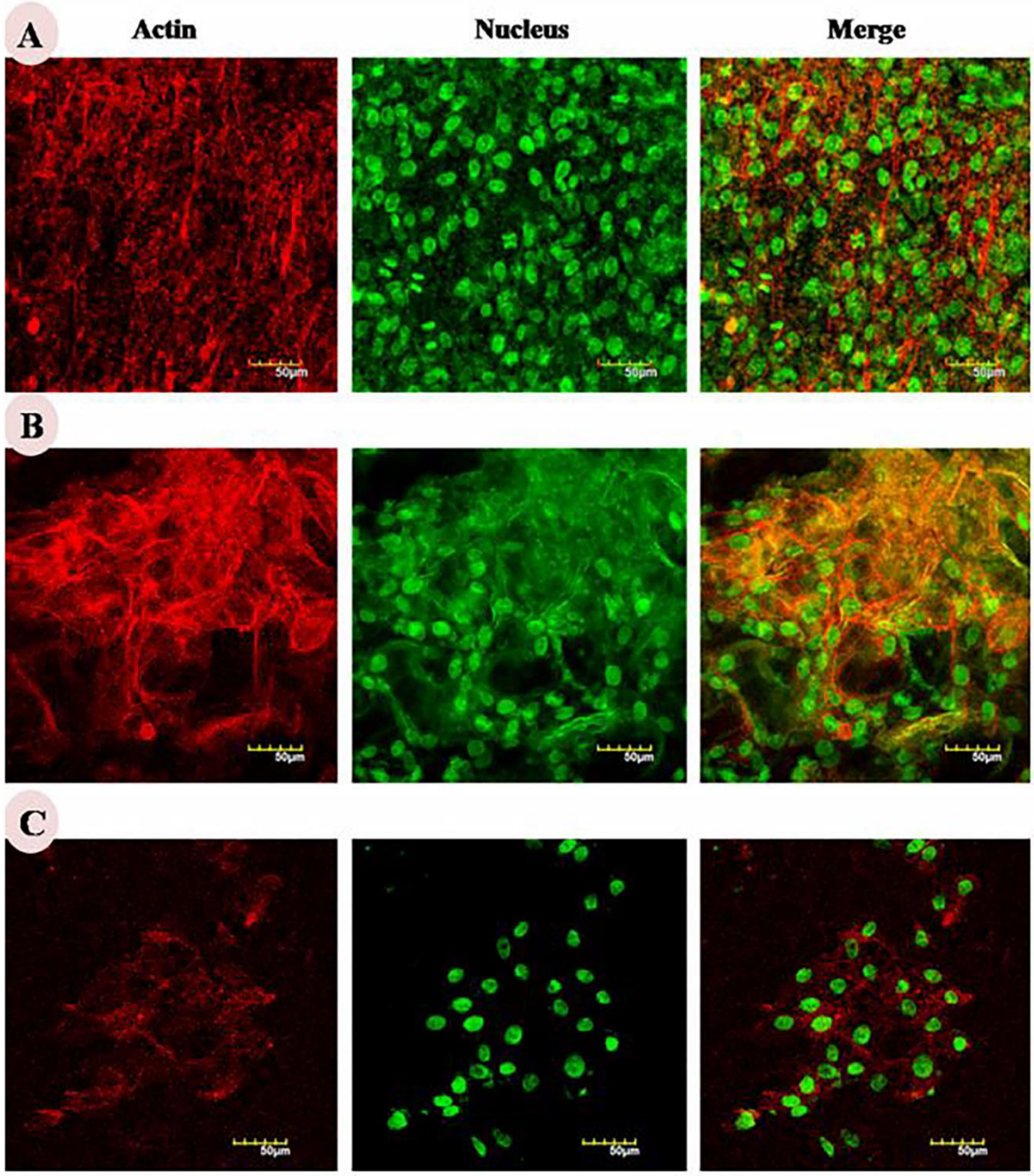

Fig 1: Confocal laser scanning images of MG-63 cells on gelatin/chitosan composite nanofibers cross-linked with Dextran aldehyde (A), Sucrose aldehyde (B) and Glutaraldehyde (C) [46].

In a recent study, Ma et al. synthesized multilayer NF mats with CS/SF and polydopamine (PDA) layers by electrospinning with a flow rate of 1 mL/h, applied voltage of 16 kV, and needle-collector distance of 16 cm [47]. Field-emission scanning electron microscopy (FE-SEM) showed increased surface roughness of the fibre mats with increasing layers of PDA from 5 to 10 and 15 layers. The addition of PDA layers to CS/SF mats increased the tensile strength from 0.29 MPa to 0.59 MPa. The contact angle of water on CS/SF mats was 56.3° compared to 41.7° for CS/SF mats with 15 layers of PDA which was attributed to the hydrophilicity of PDA. The viability and adhesion of L292 mouse fibroblasts seeded on CS/SF fibre mats increased with the addition of 15 layers of PDA and the fibre mats with 15 PDA layers had higher viability and adhesion than those with 5 or 10 PDA layers. Further, bacterial adhesion and number of bacterial colonies growing on CS/SF fibre mats decreased with the addition of 15 layers of PDA to the mats (CS/SF/PDA_{15}). Mak and collaborators investigated the effect of autoclaving on the properties of genipin crosslinked CS (CS/GN) NFs by electrospinning at an accelerating voltage of 55 kV [48]. The average diameter of CS/GN fibres reduced from 173±47nm before to 168±57 nm after autoclaving, indicating that autoclaving did not have a noticeable effect of fibre diameter. The Young's modulus of CS/GN fibres increased from 37.3 ± 3.4 MPa before autoclaving to 48.0 ± 5.8 MPa after autoclaving. Autoclaving increased hydrophilicity of CS/GN fibres as the water contact angle decreased from 33.3° ± 3.2° to 25.6° ± 3.5° after autoclaving; Autoclaving decreased enzymatic degradation of CS/GN fibres in lysozyme solution from 18.0 ± 2.2% and 14.0 ± 2.0%. The un-crosslinked CS fibres degraded faster than the crosslinked CS/GN fibres as the release of amino acids in degradation experiments, as measured by Ninhydrin assay, was faster in the un-cross

linked fibres. Shalumon et al. spun core-shell CS/SF/nHAP NFs loaded with bone morphogenetic protein-2 by electrospinning with core and shell flow rates of 0.05 mL/h and 0.3 mL/h, respectively, and an accelerating voltage of 18 kV and needle-collector distance of 12 cm. The average diameters of the core-shell NFs with thin and thick shells were 534 ± 147 nm and 346 ± 47 nm, respectively, and their corresponding shell thickness as measured by transmission electron microscopy (TEM) were 167 ± 41 nm and 101 ± 9 nm. The release of BMP-2 loaded in the shell of the NFs was higher than that loaded in the core. The loading of BMP-2 in the core-shell fibre mesh enhanced viability and growth MSCs seeded on CS/SF/nHAP or CS/SF fibres. Further, core-shell CS/SF fibre scaffolds with a thin shell and BMP-2 loaded in the core of the fibres showed highest ALP activity over 28 days of culture, demonstrating robust osteogenic differentiation of MSCs. Further, the MSCs seeded in CS/SF/nHAP scaffolds loaded with BMP-2 had highest extent of mineralization after 21 days of culture, as measured by calcium and phosphorus measurements, and highest Alizarin red staining after 28 days of culture. In addition, MSCs seeded in core-shell CS/SF/nHAP/BMP-2 fibrous composite with a thin shell showed highest expression of osteogenic markers osteocalcin (OCN), osteopontin (OPN), osteonectin (ONN) and ALP after 28 days of culture. Toskas and collaborators spun hybrid core-shell NFs with CS/PEO as the core and silica (SiO_2) as the shell by electrospinning with PS/PEO at a flow between 0.4 and 1.0mL/h, voltage between 22 and 25kV, and the needle-collector separation of 11cm [49]. The mean diameters of PEO, CS/PEO/SiO_2 (60:40), CS/PEO/SiO_2 with 50% CS/PEO and 50% SiO_2 (50:50), CS/PEO/SiO_2 (30:70), and CS/PEO/SiO_2 (70:30) core-shell NFs were 151, 88, 182, 508, and 239 nm, respectively. The CS/PEO/SiO_2 NF composites supported adhesion and growth of 7F2 mouse osteoblasts, and the cells had higher growth on 50/50% and 70/30% CS/PEO/SiO2 NFs after 6 days of culture as compared to other NF compositions. These results imply that the CS/PEO/SiO2 core-shell NFs are effective as a scaffold for bone tissue engineering. Tsai et al. added gum Arabic (GAR) to CS/GEL to reduce the solution viscosity, which resulted in higher alignment of the spun NFs [50]. The electrospinning of CS/GEL/GAR with gum Arabic was carried out using a feed rate of 0.15-0.3 mL/h, voltage of 15-30 kV, and needle-collector distance of 15 cm. The average diameter and porosity of the produced fibres were 143 ± 31 nm and 88 ± 3%, respectively. Further, Tsai et al. crosslinked the CS/GEL/GAR fibres with glutaraldehyde to improve mechanical stability of the electrospun mats, which led to 4-fold increase in tensile strength from 0.67 ± 0.15 MPa before to 2.53 ± 0.22 MPa after crosslinking. Protein deposition was used as an indirect method to assess cytocompatibility of CS/GEL NF mats before and after crosslinking. Protein deposition on CS/GEL fibres after 7 days of incubation increased from 12 μgm/cm^2 for the un-cross linked mats to 30μgm/cm^2 after 7 days of incubation. Live and dead fluorescent images of MSCs seeded on the mats showed a similar trend to the protein adsorption. Zhao et al. compared properties of carboxymethyl chitosan (CMCS) NF mats crosslinked with alginate dialdehyde (ADA) or glutaraldehyde (GA) produced by electrospinning with feed rate of 0.6 mL/h, applied voltage of 25 kV, and needle-collector distance of 15 cm [51]. The average fibre diameter ranged 200 to 400 nm. The welling ratio of CMCS/ADA and CMCS/GA fibres was 223 ± 16% and 181 ± 9%, respectively. Mouse bone marrow stromal cells (mbMSCs) seeded on the NF mats showed higher cytocompatibility and growth on CMCS/ADA mats as compared to CMCS/GA, which was attributed to the higher hydrophilicity of the ADA crosslinked CMCS NFs. Further, mbMSCs cultured on CMCS/ADA fibre mats showed higher expression of ALP osteogenic marker (9 nmol/min/mg protein) compared to CMCS/GA (6.25 nmol/min/mg protein), demonstrating higher potential of ADA crosslinked CMCS fibre mats for osteogenesis and bone tissue formation. Chen and collaborators spun core-shell NFs of CS/GEL loaded with HAP by electrospinning with a feed rate of 0.3 to 0.4 mL/h, applied voltage of 20 kV, and needle-collector distance of 12 cm followed by crosslinking the fibres with glutaraldehyde (GA) [43]. The average core diameter and shell thickness of the fibres were 150 nm and 100-200 nm, respectively. MG-63 osteosarcoma cells cultured on the CS/GEL fibres without HAP deposition had higher cell viability (87%) as compared to the fibres with HAP (79%). Further, MG-63 cells cultured on the CS-GEL fibres without HAP had higher cell attachment and spreading as compared to those fibres with HAP. This inhibition of cell attachment, spreading and viability was attributed to the calcium in HAP. Shreshta et al. synthesized composite NFs of CS with zein (ZN), which is the major corn protein enriched with glutamine, a polyurethane (PU) and carbon nanotubes (CNT) by electrospinning with feed rate of 1.0 mL/h and applied voltage of 18 kV. The addition of PU to CS/ZN increased fibre diameter from 160-260 nm to 193-360 nm, whereas the addition of CNT reduced the fibre diameter to 130 nm. The tensile strength of the composite fibres without and with CNT was 5.3 MPa and 7.5 MPa, respectively. The addition of CNT to CS/SN/PU composites increased hydrophilicity of the fibres as the water contact angle decreased from 102.0 ±1.0° without to 40.4±1.4° with CNT. According to in vitro degradation results, the mass loss of CS/ZN/PU composite fibres increased from 26% to 28% with the addition of CNT. The composite fibres with CNT showed higher adhesion, spreading and growth of MC3T3-E1 mouse calvaria osteoblasts compared to those without CNT, as measured by cell counting kit-8 (CCK-8) and FE-SEM. The addition of CNT to CS/ZN/PU composite fibres increased the expression of osteogenic markers OCN and OPN by 1.5-fold and the ALP expression by 2-fold. Based on zones of inhibition studies, the addition of CNT improved the antibacterial activity of CS/ZN/PU composite fibres. Zarei and collaborators incorporated 5-25% polypyrrole (PPY) into CS/COL/PEO fibres by electrospinning with flow rate of 0.4 mL/h, applied voltage in the range of 12-20 kV, and needle-collector distance of 12 cm [52]. Following spinning, the fibre mats were crosslinked with glutaraldehyde. The diameter of CS/COL/PEO/PPY fibres decreased from 340 nm to 84 nm as PPY increased from 5% to 25%, respectively. The tensile strength of the composite fibres ranged from 2.4 MPa to 15.0 MPa depending on COL and PPY content. Based on degradation experiments, the slowed mass loss of the composite fibres was achieved by the addition of 10% PPY. In general, adhesion, spreading and proliferation of rat MSCs was highest on CS/COL/PEO fibres without PPY, which was attributed to the natural cell compatibility of chitosan and collagen in CS/Col/PEO fibre mats. *In-vivo* experimental results using Chitosan and composite fibers fabricated using other natural polymers was depicted in Table 1.

Table 1Some invivo experiments using chitosan and composite fibers

S.N	Scaffold material	Implantation Site	Cell source	Outcome	Ref
1	CS	Rabbit calvarial bone	MG63 Cell line	CS fibrous membranes implanted at the defect site and evaluated 6 weeks post implantation, penetration of connective tissue observed in the membrane, 29% new bone formation in CS membranes compared to 10% in the control, defect site in CS group covered with new bone whereas new bone at the edges of defect in control group, no implant degradation observed after 6 weeks implantation.	88
2	CS	Mouse femur	No in-vitro studies	CS nanofibers (200 nm diameter) implanted in the left femur and compared with empty defect in right femur, no sign of hepatotoxicity or nephrotoxicity 21 days post implantation by histological analysis, accelerated bone healing observed in the CS NFs implanted femur by micro CT and x-ray scanning as compare to the control, increase in trabecular bone thickness in the CS NFs implanted femur by histomorphometric analysis, elevated expression of Runx2 (20-fold), ALP (1.5-fold) and OCN (1.8-fold) in the CS NFs implanted femur as compared to the control.	89
3	CS microfibers	Rat subcutaneous implantation	Rat muscle-derived stem cells (rMDSCs)	Analysed 4 weeks post implantation, intensity of H&E staining images for host cells at the site of implantation higher in CS/rMDSC NFs implants CS NFs, increased vascularization and decreased immune response (macrophages) in CS/rMDSCs NFs implant compared to NFs.	90
4	CS/collagen nanofibers	Rabbit calvarial bone	Rabbit MSCs	In-vivo bone formation in CS/nano electrospun collagen and CS/solid wall collagen membranes assessed, both scaffold types did not invoke inflammatory response in rabbit after 8 weeks implantation, scaffolds with electrospun coating produced new bone of 48.47±6.78 mm^2 whereas solid wall collagen coating produced 16.83±4.2 mm^2, bone growth spread throughout the defect in CS/nano electrospun collagen but restricted to scaffold edges in CS/solid wall collagen membrane.	88
5	Triethylamine acetone and di-tert-butyl dicarbonate treated CS fibrous membrane (TDCF)& commercially available Collagen membrane as control	Sprague-Dawley rat calvarial bone	Saos-2 human osteoblasts	histological studies showed increased percentage of new bone volume to defect volume after 3 months implantation with 24.8±6.5% and 36.6±16.2% for collagen and chitosan fibrous membranes, respectively, micro-CT analysis revealed no difference between the two groups with respect to bone density and percentage of new bone volume to defect volume, new bone surface area to new bone volume was slightly higher in collagen (17.1±2.6%) as compared to CS (15.1±2.7%), both scaffolds showed minimal inflammatory response.	91

1.4 Chitosan Based Nanofibers With Synthetic Biopolymers

Tabaei and collaborators investigated the role of surface modification by plasma treatment on the properties of CS/PEO/coral composite NFs [53]. The fibres were produced by electrospinning using a flow rate, applied voltage and needle-collector distance of 0.2-0.7 mL/h, 26 kV, and 18 cm, respectively. The produced NFs were plasma treated and their water contact angle was measured as related to wettability. Plasma treatment reduced the contact angle of CS/PEO/coral fibres from 33-59° range prior to treatment to 12.6+1.5° after treatment, implying higher hydrophilicity of the plasma treated fibres. The addition of coral to CS/PEO fibres reduced the tensile strength of the fibres from 4.8 to 1.1 MPa before plasma treatment and 1.8 to 1.3 MPa after plasma treatment. Plasma treatment increased viability and compatibility of the fibres with MC3T3 mouse calvaria osteoblast precursor cells and accelerated the formation of apatite crystals and mineralization, as imaged by SEM. The improved hydrophilicity, cell compatibility and mineralization of plasma-treated CS/PEO/coral fibres demonstrate their potential value as a scaffold in bone tissue engineering. Further, the authors investigated the effect of type of gas used during plasma treatment, namely nitrogen, argon and mixture of helium and ammonia (N_2, Ar, He/NH_3), on morphology, wettability, and cell biocompatibility. The density of hydrophilic

groups was highest on N_2 and He/NH_3 plasma-treated NF surfaces followed by Ar plasma-treated NFs. The water contact angles of N_2, He/NH_3, and Ar plasma-treated NF surfaces were 10.6±2.0°, 23.7±3.2° and 57.0±0.2°, respectively. The leaching of PEO from CS/PEO/coral NFs after electrospinning and plasma treatment in SBF was relatively high for He/NH_3 and Ar treated fibres (7.4-8.5 µMol/L) and low for N_2 treated fibres. The interaction and adhesion of human foreskin fibroblasts (HFF) cultured on Ar plasma treated CS/PEO/coral NFs was higher than those plasma treated with N_2 and He/NH_3, which was attributed to the density of functional groups on these surfaces. Balagangadharan and collaborators investigated the use of a plant-based phenolic compound sinapic acid (SPA) loaded in CS nanoparticles (CS-SPA NPs) and the NPs incorporation in polycaprolactone (PCL) NFs for use as a bone tissue scaffold [54]. The complex hydrophobic nature of SPA makes it useful in assembling NPs by ionic gelation with CS with SPA concentrations ranging from 20 µM and 100 µM. The feed rate, applied voltage, and needle-collector distance in electrospinning CS-SPA NPs in PCL were 1 mL/h, 10 kV, and 10 cm, respectively. The percent of SPA delivered from the fiber-embedded CS-SPA NPs in SBF for SPA concentration of 20, 50 and 100 µM was 43%, 53% and 60, respectively. Therefore, the fiber embedded NPs can be used as a carrier for efficient delivery of SPA in drug delivery applications. There was no noticeable difference in the viability of mouse MSCs cultured on CS-SPA NPs in PCL fibrous scaffolds with different concentrations of SPA in the NPs. However, the scaffold with 50 µM SPA NPs showed highest ALP activity and expression of osteoblast differentiation markers (COL-1, OCN) by the cultured MSCs as compared to other SPA loadings. **Figure 2** depicts fast healing of defects in drug loaded scaffolds as compared to scaffolds without drugs

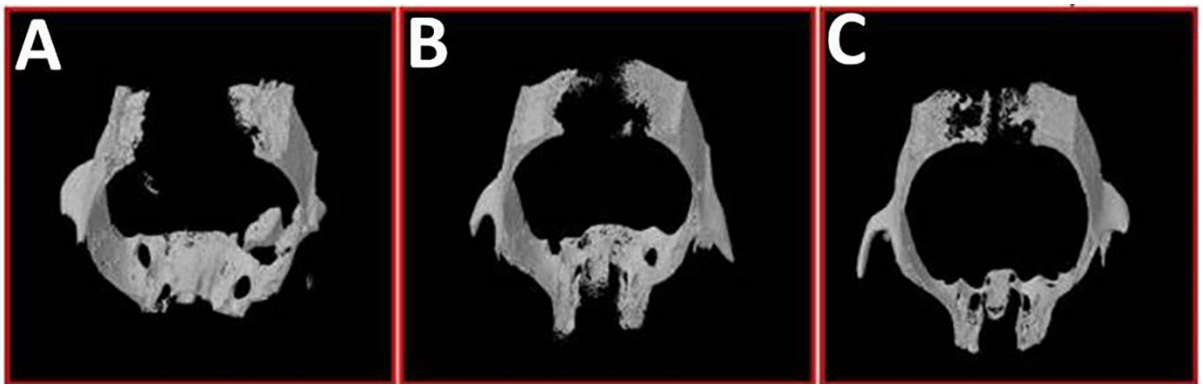

Fig 2: Differential Healing of Calvarial bone defects in control (A), Chitosan/PCL (B) and drug loaded Chitosan/PCL nanofibers (C). Fast healing was observed in drug loaded Chitosan/PCL nanofibers (C) groups as compared to other groups (A&B) [54].

Villegas et al. produced composite CS/PEO NFs doped with zinc oxide (ZnO_2) NPs with sizes in the range of 60-100 nm by electrospinning followed by crosslinking the spun fibers with ultraviolet (UV) crosslinking using pentaerythritol triacrylate (PETA) photo-initiator [55]. The electrospinning of the aligned fibers was carried out with a flow rate of 0.4 mL/h, applied voltage of 25 kV, needle diameter of 1.02 cm, needle-collector distance of 20 cm, and collector rotation speed of 200 RPM. The mean diameter of the produced fibers was 150-450 nm. The effect of duration of UV crosslinking on properties of the produced fibers was investigated at a radiant flux of 4.77 W/cm^2 for radiation times of zero to 120 min. The CS/PEO/ZnO fibers UV crosslinked for 100 min showed highest swelling capacity in aqueous solution at 770% swelling. The zone of inhibition of UV-crosslinked CS/PEO/ZnO NFs against *S. aureus, E. coli, S. epidermidis and P. aeruginosa* bacterial strains was 11.0±0.3, 13.0±0.3, 12.0±0.3 and 13.0±0.3 mm, respectively, as measured by the disc dilution method with chlorhexidine as the positive control and crosslinked CS/PEO NFs as the reference. Goudarzir et al. investigated the effect of electrospinning parameters on the properties of composite fibers based on CS, polyvinyl alcohol (PVA), and sericin (SCN) which is a protein formed in the production of silk (CS/SCN/PVA). [56]. These parameters included applied voltages in the range of 15-30 kV and needle-collector distances of 10 and 15 cm while the needle diameter and solution feed rate were maintained constant at 0.5 mm and 0.25 mL/h, respectively. The NFs spun at a needle-collector distance of 10 cm had a larger mean diameter compared to those at 15 cm. Conversely, there was greater jet instability and fraction of bead-like fiber deposition at a needle-collector distance of 10 cm. The NFs spun at an applied voltage in the 22-27 kV range had the lowest mean diameter at a constant needle-collector distance of 10 cm as compared to voltages outside of the above range. Next, the authors prepared CS/SCN/PVA composite NFs containing 1 wt% silver nitrate ($AgNO_3$) bye electrospinning at the optimized needle-collector distance of 10 am and an applied voltage of 22 kV and evaluated for antibacterial activity using gram-negative E. Coli. The bacterial activity of E. Coli cultured on CS/SCN/PVA mesh reduced to zero upon the addition of 1 wt% $AgNO_3$ to the fibers as compared to $3.5x10^5$ CFU/mL bacterial activity for CS/SCN/PVA fibers without $AgNO_3$. Further, the addition of AgNO3 to the fibers reduced the mean diameter of the fibers to 95 nm. Jin et al. investigated antibacterial activity of CS and calcium phosphate (CaP) NFs loaded with silver particles prepared by electrospinning with a feed rate of 1.0 mL/h, applied voltage of 26 kV, and needle-collector distance of 20 cm [57]. The silver NPs were uniformly distributed in the fibers as confirmed by mapping by energy dispersive spectroscopy (EDS). Based on in vitro release studies, there was robust release of physically absorbed silver ions (>76%), as opposed to doped silver ions, from the CaP/CS NFs to SBF. According to SEM images, there was gradual deposition of apatite crystals on the surface of NFs with incubation time in SBF, which would be beneficial to bone regeneration. The silver-loaded CaP/CS NFs reduced the attachment and growth of *P. gingivalis* and *S. mutans* on the surface of the fibers in suspension culture. Although the presence of CaP facilitated adhesion of mouse MSCs on the surface of NFs, the release of silver ions hindered growth

of the MSCs. The CaP/CS NFs with 0.114% Ag was found to be the best composition for supporting both osteogenesis of MSCs as well as inhibition of bacterial activity. Sambudi et al. synthesized calcium carbonate (CaC) loaded CS/PVA NFs to mimic the mineral structure of bone tissue nu electrospinning with flow rate of 10 µL/min, applied voltage of 15 kV, and tip-target distance of 15 cm [58]. The addition of ellipsoidal-shaped calcium carbonate particles increased the average diameter of NFs from 71.5 ± 23.4 nm to 282.0 ± 51.0 nm which improved tensile strength of the NFs from 16 ± 3 MPa to 432 ± 94 MPa. The CaC loading did not affect the contact angle or hydrophilicity of the NFs. Satpathy et al. produced CS/PVA NF meshes loaded with HAP NPs (CS/PVA/nHAP) by electrospinning using a flow rate of 1 mL/h, applied voltage in the range of 20-25 kV tip-collector distance of 14 cm [59]. The mean diameter of the NFs was reduced by the addition of nHAP from 395±162 nm to 300±121 nm. The contact angle of the fibers decreased to 12.53°±0.25° after nHAP addition, which improved wettability of the fibers. The degree of swelling of CS/PVA/nHAP fiber meshes in aqueous solution was 194% which was higher than CS/PVA and PVA fiber meshes at 142% and 130%, respectively. The mass loss of CS/PVA/nHAP meshes after 1 and 7 days of incubation in SBF was 13% and 30%, respectively, which was higher than CS/PVA meshes at 6% to 21%. The cell viability and growth of mouse MC3T3 precursor osteoblasts seeded on CS/PVA/nHAP fiber meshes were higher than those seeded on CS/PVA meshes, demonstrating higher usefulness of CS/PVA/nHAP fibers in regenerative medicine. Toloue et al. prepared NFs based on a blend of CS and polyhydroxybutyrate (PHB) loaded with alumina nanowires(CS/PHB/nwALO) by electrospinning at a flow rate of 0.6 mL/h, applied voltage of 22 kV, and needle-collector distance of 25 cm [60]. The mean diameter of CS/PHB/nwALO fibers increased from 480 to 650 nm with increasing nwALO content from 1 to 5 wt%, respectively, as compared to those of CS/PHB fibers with 320 and 430 nm. Further, the surface roughness of CS/PHB fibers noticeably increased with the addition of nwALO from 346±23nm without nwAL to 492±67nm with nwALO. The addition of 3 wt% nwALO to CS/PHB fibers increased wettability as the water contact angle decreased from 54±1° to 30±1°. However, the contact angle of the fibers decreased for nwALO contents higher than 3 wt%. The tensile strength of composite CS/PHB fiber meshes with 3 wt% nwALO was 11.2 ± 1.2 MPa which was higher than the composites with other nwALO percentages (1.8 to 6.4 MPa), and higher than PHB and CS/PHB fibers with values of 2.8±0.2 MPa) and 0.9±0.3 MPa, respectively. The degradation of CS/PHB fiber meshes slowed with the addition of nwALO based on studies in SBF over 100 days. Further, optimum cell viability, adhesion, and osteogenic differentiation of MG-63 osteosarcoma cells was achieved when seeded on CS/PHB composite fiber meshes was 3 wt% nwALO. Talebian et al. investigated the properties of composite bioglass-loaded CS/PEO (CS/PEO/BG) NFs produced by electrospinning with a flow rate of 0.4 mL/h and needle-collector distance of 10 cm [61]. The tensile strength and rupture strain of CS/PEO/BG nanofiber composites was 3.0±0.2 MPa and 4%, respectively, which was slightly higher than that of CS/PEO fibers at 1.6±0.2 MPa and 2.5%. The addition of bioglass to CS/PEO NFs improved hydrophilicity of the scaffolds as the water contact angle decreased from 58±4° for CS/PEO NFs to 38.1±2.0° for CS/PEO/BG NFs. Human MSCs seeded on CS/PEO/BG NFs deposited higher amounts of plate-like apatite crystals with an average thickness in the range of 100-150 nm with 2-fold higher ALP activity as compared to those NFs without bioglass. In another study, Saatchi et al produced CS/PEO/BG NFs doped with 10-40 wt% cerium (CS) using electrospinning with a flow rate of 0.2 mL/h, applied voltage of 17 kV, and needle-collector distance of 23 cm [62]. The average fiber diameter was in the range of 86-140 nm and fiber size increased with bioglass content. Energy dispersive X-ray analysis confirmed the presence of cerium-doped bioactive glass (dCe-BG) in the NFs, which improved hydrophilicity of the fibers as the contact angle decreased from 71° to 53° with Ce doping. The viability of 3T3 mouse fibroblasts seeded on CS/PEO/BG/dCe NFs was independent of BG content. However, the NFs with 30 wt% BG showed improved cell morphology, spreading and adhesion as compared to other BG contents. Govindasamy et al. investigated the effect of incorporation of aluminosilicate clay mineral halloysite (HAL-72, 154 nm average size) on the properties of CS/PEO NFs produced by electrospinning with up to 10% HAL content, flow rate of 1.2 mL/h, applied voltage of 19-26 kV, and needle-collector distance of 15 cm [63]. As the HAL content was increased to 5 wt%, pore size of the NF meshes increased from 105 to 155 nm and tensile strength from 7 to 26 MPa, followed by a decrease for HAL contents above 5 wt%. HAL reduced wettability of the NFs because as HAL content increased to 10 wt%, the water contact angle increased from 27±5° (no HAL) to 94±11°. The viability and adhesion of human osteoblasts was higher on CS/PEO/HAL NFs with 5 wt% HAL with ALP content of 0.6 nmol/day/mg as compared to other HAL contents with ALPs in the range of 0.3-0.5 nmol/day/mg. The results indicated that the NFs with 5 wt% HAL would be best suited for bone regeneration applications. Ahmadi et al. investigated the effect of laponite (LPT) addition on the properties of PCL/CMCS composite NFs produced by electrospinning with flow rate of 0.4 mL/h, applied voltage of 25 kV, and needle-collector distance of 15 cm [64]. The fiber diameter increased from 390 nm to 470 nm by the addition of LPT to the fibers whereas water contact angle decreased from 32° decreased to <10°, implying increased fiber wettability with LPT addition. The viability of human bone marrow derived MSCs seeded on PCL/CMCS meshes with 3.5% LPT was higher than those seeded on PCL/CMCS or PCL NFs and the cells exhibited elongated morphology on PCL/CMCS/LPT NFs. Further, the MSCs seeded on PCL/CMCS/LPT NFs and cultured in osteogenic medium without an osteogenic differentiation factor stained strongly for Alizarin red, indicating production of mineralized matrix, 2-fold increase in calcium content, and 1.5-fold increase in ALP activity. In addition, immunohistochemical staining of the MSCs revealed noticeably higher expression of ONN on PCL/CMCS/LPT NFs as compared to those cells on PCL/CMCS or PCL NFs. These results suggest that LPT has osteoinductive properties and could potentially be used as an alternative to bone morphogenetic proteins (BMPs) and TCP in bone regeneration. Fadaie et al. incorporated CS nano fibrils (nfCS) into PCL NFs by electrospinning with PCL and nfCS concentrations of 10-12 wt% and 1-10 wt% in the electrospinning solution, respectively, solution flow rate of 2.5 mL/h, applied voltage of 18 kV, and needle-collector distance of 14 cm [65]. The average fiber diameter of the NFs varied from 160±88 nm to 800±433 nm. The NFs with 8 wt% PCL and 10 wt% nfCS produced meshes with highest tensile strength of 6.0±0.7 MPa and lowest water contact angle of 84±1°. The NFs with 10 wt% nfCS showed improved

adhesion and spreading of the seeded normal human dermal fibroblasts as compared to other fiber compositions, as measured by lactate dehydrogenase (LDH) activity of the cells. Yang et al. synthesized CS/PVA/GO NFs by electrospinning using an applied voltage of 23 kV and needle-collector distance of 15 cm [66]. The average diameter of the synthesized NFs was 83 ± 10 nm and the fiber diameter increased with increasing GO content. The addition of GO to the NFs increased wettability as the water contact angle decreased from 68° for NFs with no GO to 22° for 5 wt% GO NFs. The addition of 5 wt% GO improved antibacterial activity of CS/PVA/GO NFs as measured by the zone of inhibition against *Escherichia coli* and *Staphylococcus aureus* bacteria. Topsakal et al. encapsulated the antibacterial agent amoxicillin (AMX) in composite fibers based on CS, beta-tricalcium phosphate (β-TCP), and a polyurethane (CS/β-TCP/PU) by electrospinning with a flow rate of 1-2.3 mL/h, applied voltage of 27-31 kV, and needle-collector distance of 15 cm [67]. The addition of 3 wt% CS and 5 wt% β-TCP to 15 wt% PU (CS3/ β-TCP5/PU15) spinning solution produced composite NFs with highest tensile strength of 7.8 MPa as compared to other NF compositions, which was 7-fold higher than that of PU NFs without CS or β-TCP with a tensile strength in the range of 1.1-1.7 MPa. The adhesion of L929 mouse fibroblast cells to the composite CS/β-TCP/PU NFs was significantly higher (75-80%) as compared to PU NFs, and the cell viability and growth was highest on CS3/β-TCP5/PU15 NFs. Further, the optimum loading efficiency of 62% and release after 24 h of 68% for AMX was observed on CS3/β-TCP5/PU15 NFs. The bone regeneration potential of PCL/carboxymethyl cellulose (PCL/CMC) produced by electrospinning was investigated by Sharifi et al. and compared with that of PCL/CS NFs [68]. The flow rate, applied voltage, and needle-collector distance in the electrospinning process had ranges of 0.1-0.7 mL/h, 18-30 kV and 16-20 cm, respectively. The average diameters of PCL/CS and PCL/CMC NFs with 5 wt% CS or CMC were 450 and 470 nm, respectively, which was much higher than that of PCL fibers at 200 nm. The water contact angle on PCL/CS and PCL/CMC NFs decreased with increasing CS or CMC concentration. The contact angles for PCL/CS NFs and PCL/CMC were in the range of 92-112° and 51-58°, respectively, which were lower than that of PCL at 123°. The PCL/CMC composite with 15 wt% CMC produced most hydrophilic NFs with contact angle of 51±3°. The human MG-63 osteoblasts showed higher viability and growth on PCL/CS or PCL/CMC NFs with 10 wt% CS or CMC compared to other NF compositions. Su et al. investigated the effect of coating polylactide (PLA) nanofibers with chitosan/calcium silicate (CS/CaSi) on their use as a scaffold in bone tissue regeneration [69]. The PLA NFs were produced by electrospinning using a 5 mL syringe with injection rate of 0.5 mL/h, applied voltage of 21 kV, and needle-collector distance of 18 cm. Following electrospinning, the PLA NFs were soaked in CS/CaSi solutions of different concentrations to coat the NFs. The water contact angle on CS/CaSi coated PLA NFs decreased from 91 ± 4° for 0.05 wt% CS to 79 ± 3° and 35 ± 2° for 0.1 and 0.15 wt% CS, respectively, showing direct relation between hydrophilicity and CS content of the coating. Great HAP deposition from SBF was observed for the coated PLA NFs with 0.15 wt% CS. The mass loss of coated NFs with 0.15 wt% CS was 25% after 8 weeks of incubation as compared to other coating compositions which was in the range of 8-22%. Further, adhesion and proliferation of human MSCs was higher on the coated NFs with 0.15 wt% CS as compared to other coating compositions. The adsorption of COL-I and fibronectin (FN) from solution onto the surface of coated NFs with 0.15 wt% CS was higher than the NFs with other coating compositions. Further, the expression of osteogenic markers ALP, OPN, and OCN by the MSCs seeded on CS/CaSi coated PLA NFs with 0.15 wt% CS was 1.7-fold, 1.3-fold, and 1.4-fold higher than the coatings with other compositions. Song et al. investigated antibacterial activity of CS/PEO NFs loaded with $AgNO_3$ and chlorhexidine (CHX) [70]. CS/PEO NPs loaded with up to 5 wt% $AgNO_3$ was produced by electrospinning with a flow rate of 4 mL/h, applied voltage of 27 kV, and needle-collector distance of 15 cm. The membranes were then cut into discs and soaked in CHX solutions of different concentrations for CHX loading. The average diameter of the NFs was in the range of 90-120 nm. The delivery of CHX from the NF disks was burst release whereas that of $AgNO_3$ was sustained release with incubation time in SBF. The NFs with CHX concentrations >25 µg/mL were cytotoxic whereas Ag+ concentrations up to 50 µg/mL in the NFs did not show toxicity. The NF disks with 5 wt% AgNO3 and 20-60 µg/disk CHX showed visible inhibition zones against *S. aureus*, indicating that the $AgNO_3$/CHX loaded CS/PEO NFs possess considerable antibacterial activity. **Table 2** illustrates results of in-vivo experiments using Chitosan and its composite fibers prepared by using synthetic polymers.

Table 2 In-vivo experiments using Chitosan and its composite fibers prepared by using synthetic polymers.

S.N	Scaffold material	Implantation Site	Cell source	Outcome	Ref
1	CS/PCL	Subcutaneous implantation in albino mouse (BALB/cJZtm)	No significant *in-vitro* studies	Lesser recruitment of leukocytes in CS blended PCL nanofibers with limited to no inflammatory responses up to 2 weeks post-implantation, cell infiltration and collagen deposition by H&E and Van Gieson staining showing the role of CS in PCL NFs, detection of CD31 marker shows potential for vascularization in the composite NFs.	92
2	N-methylene phosphonic chitosan/ PVA (NMPC/PVA)	Rabbit tibia	MG-63 pre osteoblast cells	Newly formed collagen assessed by Van Geisson staining and radiological imaging have shown improved new bone formation in NMPC/PVA as compared to PVA NFs, composite fibers showing enhanced bone formation compared to PVA NFs.	93
3	Polypropylene carbonate/CS	Rabbit femur	Bone marrow mesenchymal	CS NFs introduced in porous PPC scaffold matrix as a mimic to the natural bone, the PPC and PPC/CS	94

	(PPC/CS)		stem cell (BMSCs)	both showing new bone formation at the implanted site, but new bone spread to the entire defect in the composite NFs as compared to PPC NFs only, osteogenesis rate higher on PPC/CS composite scaffolds as compared to PPC after 4-months post implantation showing accelerated osteogenesis and healing.	
4	CS/Polybutylene succinate	Subcutaneous implantation in Wistar rats	No in-vitro studies	Scaffolds showed inflammation at the defect site in the first 6 weeks but subsided 12 weeks post implantation, no inflammation observed in CS and CS/Polybutylene implants, H&E staining showed formation of neobone at the margins of the defect in control whereas complete covering of the defect in CS/polybutylene succinate scaffolds, higher collagen deposition (Masson's trichrome) and vascularization (expression of α-smooth muscle actin) observed in the composite scaffold, both scaffold groups maintained their integrity after 3 months of implantation.	[95]
5	CS/PLGA	Rabbit calvarial bone	No in vitro studies	Effect of PLGA on CS fibrous membranes assessed with respect to defect closure and formation of new bone, defect closure and new bone formation was higher in membranes with 1 and 0.5 wt% PLGA 2 months post implantation with corresponding values of 3.4±1.56 mm and 1.46±0.44 mm as compared to other scaffold groups.	[96]
6	PCL/nano CS/sinapic Acid	Rat calvarial bone	Mouse MSCs	PCL/nano CS fibers loaded with varied concentrations (20, 50 and 100 μM) of plant extract Sinapic acid (osteoblast modulator), fibers with 50μM sinapic acid used for in-vivo studies based on superior physicochemical, mechanical and in-vitro biocompatibility, new bone formation analysis via micro-CT images showed PCL/nCS fibres loaded with 50 μM SA with increased neobone formation when compared to PCL/nCS fibres, bone volume to tissue volume (quantitative analysis) was 15 for PCL/nCS/SA as compared to 9 for CL/nCS fibers, qualitative analysis of new bone and collagen deposition by H&E staining and Manson's trichrome assay showed increased bone quality and collagen in PCL/nCS/SA fibres as compared to its counterpart which was attributed to the addition of SA and expression of RunX-2 and enhancement of differentiation of the seeded mMSCs leading to fast bone remodelling.	[54]
7	CS/PEO	Subcutaneous implantation in Wistar rats	Human fetal foreskin fibroblast cells	The healing of wound area was 16% with CS/PEO fibers whereas it was 4.5% in the control group (without fibers), fast re-epithelialisation led to new tissue formation, H&E staining images showed less inflammation on CS/PEO scaffolds as compared to control group.	[97]

1.5 Composites Of Chitosan With Ceramics

Januariyasal et al. incorporated varied amounts of carbonated hydroxyapatite (CHAP) in CS/PVA NFs by electrospinning with a feed rate of 0.25 mL/h, applied voltage of 15 kV, and needle-collector distance of 12 cm [71]. Morphological analysis with SEM revealed a decrease in fibre diameter with increasing CHAP content. CHAP additions higher than 15 wt% resulted in aggregation of ceramic particles which led to morphological disruption of the fibrous scaffold. The average diameter of CHAP incorporated NF matrices was in the range of 130-160 nm and the ultimate tensile strength was in the 5.5-7.5 MPa range. As the CHAP content of the CS/PVA NFs was increased from 5 wt% to 10, 15 and 20 wt%, protein adsorption (based on the weight of NFs) on the scaffolds with incubation in fetal bovine serum (FBS) increased from 1.0% to 1.5, 1.8 and 2.2%, respectively. As the CHAP content was increased, viability of MC3T3-E1 osteoblasts seeded on CS/PVA scaffolds increased, and the scaffold with 20 wt% CHAP showed highest cell viability and protein adsorption. Considering aggregation at high CHAP loading, the NFs with 15 wt% CHAP was the most suitable CS/PVA/CHAP fibrous scaffold for bone tissue regeneration. Hokmabad et al. produced PCL/PEG/PCL NFs with or without CS by electrospinning and investigated the effect of addition of silica or HAP NPs to the fibres on the

morphology, hydrophilicity, tensile strength, and osteogenesis of human dental pulp stem cells (hDPSCs) [72]. Fibre diameter increased with increasing silica or HAP content. The addition of silica or HAP to PCL/PEG/PCL/CS NFs increased fibre diameter from 200 nm to 260 nm and 230 nm, respectively, which was attributed to a reduction in conductivity of the spinning solution with silica or HAP addition. The tensile strength of the fibres increased from 2.8 MPa to 4.0-6.0 MPa with the addition of silica and 6.0-11.0 MPa with the addition of HAP. The addition of silica or HAP to the fibres increased mass loss slightly from 8% after 6 weeks incubation in SBF to 11-12% and 9-10%, respectively. Coating the BFs with silica considerably reduced the water contact angle from 126º for PCL/PEG/PCL/CS NFs without coating to 110º for HAP coated and 70º for silica coated NFs, which was attributed to higher hydrophilicity of silica NPs. The viability and spreading of hDPSCs was higher on PCL/PEG/PCL/CS NF scaffolds coated with 15 wt% HAP as compared to silica coated scaffolds. Further, the expression of osteogenic differentiation markers BMP-2, Runx-2, DSSP, and OCN as well as Alizarin red staining of hDPSCs seeded on PCL/PEG/PCL/CS scaffolds coated with 15 wt% HAP was higher than the 15 wt% silica coated or uncoated PCL/PEG/PCL/CS scaffolds. Frohbergh and collaborators produced composite NF scaffolds of CS/HAP crosslinked with Genipin (CS/HAP/GN) NFs by electrospinning at a flow rate of 1.2 mL/h, applied voltage of 15 kV, and needle-collector distance of 15 cm [73]. Genipin crosslinking of CS/HAP NFs increased fibre diameter from 230 ± 154 nm (no crosslinking) to 335 ± 120 nm. The addition of HAP to un-cross linked matrices did not affect the Young's modulus whereas 1 wt% HAP addition to crosslinked matrices increased the modulus from 77 ± 9 MPa to 143 ± 13 MPa. The cell viability, ALP activity, and expression of osteogenic differentiation markers of immortalized mouse 7F2 osteoblasts cultured on CS/HAP/GN scaffolds were higher than those cultured on CS/GN scaffolds after 21 days of incubation. Zhang and collaborators produced composite chitosan NF scaffolds with 30 wt% HAP and 20 wt% PEO doping ratio (CS/PEO/HAP) using electrospinning with a flow rate of 1.2 mL/h, voltage of 17.5 kV and needle-collector distance of 34 cm [74]. The composite NFs had a uniform diameter of 214 ± 25 nm which was higher than the CS NFs at 138 ± 15 nm, as measured by SEM imaging. The mineralized ECM production by human fetal osteoblasts (hFOBs) cultured on CS/PEO/HAP scaffolds were lower than the control TCP scaffolds after 5 days of incubation, which was attributed to prevention of protein adsorption by PEO in the scaffolds. However, the growth of hFOBs cultured on CS/PEO/HAP scaffolds was 43% and 110% after 10 and 15 days of incubation, respectively, as compared to CS scaffolds with 29% and 90% cell growth. Zhang et al. prepared CS/PHBV/HAP nanofibrous scaffolds by electrospinning at a flow rate of 1mL/h, applied voltage of 13 kV and needle-collector distance of 10-15 cm [75]. Fiber diameter was found to decrease with increasing HAP content (2-8 wt%) in the range of 2-8 wt% with average diameter of 400 ± 70 nm and 260 ± 110 nm at 2 and 8 wt%, respectively. The water contact angle decreased from 126 ± 1º to 79 ± 2º for HAP content of 2 and 8 wt%, respectively. The tensile strength of CS/PHBV/HAP scaffolds with 8 wt% HAP was 151±2 MPa which was higher than the scaffolds with 4 wt% HAP at 102±5 MPa. The growth of hFOBs cultured on CS/PHBV NFs was 39% more than that of virgin PHBV NFs whereas the growth for CS/PHBV/HAP NFs with 4 and 8 wt% NFs was 24% and 34%, respectively. Further, the ALP activity of hFBOs cultured on PHBV/CS/HAP NFs with 8 wt% HAP was higher than other HAP compositions after 3 weeks of incubation, suggesting this composition is best suited for mineralized tissue regeneration. Zhang and collaborators spun CS/HAP/COL NFs with up to 7 wt% COL by electrospinning at a flow rate of 2.0 ml/h, applied voltage off 28 kV, and needle-collector distance of 22 cm [76]. The average fiber diameter was 180±30 nm, with aligned morphology and the incorporation of HAP in the fibers was validated by FE-SEM. The tensile strength of pristine CS NF meshes was 7.7±0.8 MPa) which was higher than that of CS/HAP at 4.4±0.7 MPa and CS/HAP/COL at 2.6±0.4 MPa. In contrast to tensile strength , the growth and mineralized ECM deposition, and ALP activity of hFOBs cultured on CS/HAP/COL scaffolds were 35%, 22%, and 44% higher than those hFOBs cultured on CS/HAP scaffolds without collagen or virgin CS scaffolds. Zhao and collaborators prepared CMCS/PEO and CMCS/HAP nanofiber meshes by varying the molecular weight (MW) of PEO or applied voltage [77]. Next, the mineral content of the CMCS/HAP meshes were increased 5-fold by immersion in SBF. The diameter of CMCS/PEO fibers with PEO MW of 300 kDa changed slightly from 990±430 nm to 960±480 nm as the applied voltage was increased from 13 to 18 kV, and the diameter changed from 660±270 nm to 420±130 as the PEO MW was increased from 600 kDa to 1000 kDa at constant voltage of 25 kV, indicating that the PEO MW had a considerable effect on fibre size and morphology. The growth of mouse bone marrow MSCs (mBMSCs) cultured on CMCS/HAP meshes was higher than those cultured on CMCS/PEO. Further, the mRNA expression of osteogenic markers ALP, Runx-2 and OCN of mBMSCs cultured on CMCS/HAP meshes were 10-fold, 5-fold and 1.5-fold higher on CMCS/HAP meshes as compared to those cultured on CMCS/PEO. These results suggested the suitability of CMCS/HAP scaffolds for bone regeneration. Shalumon and collaborators developed biomimetic scaffold based on CS/CL loaded with nano-bioglass (CS/PCL/nBG) or nano-HAP (CS/PCL/nHAP) using electrospinning with an applied voltage of 18 kV and 10 cm needle-collector distance [78]. The fibre diameter was in the range of 100-200 nm for nBG and nHAP loaded fibres. Fibre meshes with 3 wt% nGB or nHAP showed higher protein adsorption than other nBG or nHAP compositions. The MG-63 osteoblasts and human periodontal ligament fibroblasts (hPDLFs) were used to evaluate viability, adhesion, and differentiation of cells cultured on the fibre meshes. The viability, adhesion and osteogenic differentiation of both cell types was higher on CS/PCL/nHAP and CS/PCL/nBG NFs with 3 wt% nHAP or nBG as compared to CS/PCL NFs with 1.5 wt% nHAP or nBG. Pangon et al. produced CS/PVA, CS/PVA/chitin whiskers (CS/wCTN), CS/PVA/HAP, and CS/PVA/HAP/wCTN NF meshes by electrospinning using a feed rate, voltage and distance of 0.05 mL/h, 18 kV and 15 cm, respectively [79]. Next, the prepared fibres were crosslinked with Glutaraldehyde to improve fibre stability. Fiber diameter was found to decrease from 194 nm to 96 nm with increasing chitin whisker content. Tensile strength decreased by the addition of chitin whiskers from 1.3 MPa to 0.8 MPa. However, HAP addition to the fibres improved the tensile strength from 1.3 MPa to 2.1 MPa. The compatibility and cell-fibre interaction for mouse MC3T3-E1 calvaria cells cultured on HAP containing NF meshes (CS/PVA/HAP or CA/PVA/wCTN) was higher as compared to those meshes without HAP (CS/PVA or CA/PVA/wCTN), indicating the

importance of HAP in cytocompatibility of CS/PVA scaffolds. Talebian et al. prepared BG incorporated CS/PEO (CS/PEO/BG) NFs by electrospinning using a feed rate of 0.4 mL/h, applied voltage 6 kV and needle-collector distance of 10 cm [61]. The average fibre diameter increased by 100-150 nm after BG incorporation. The incorporation of BG increased hydrophilicity of CS/PEO NFs as the water contact angle decreased from 57.5º to 38.1º with BG addition. The tensile strength of CS/PEO NF meshes increased from 1.6±0.2 MPa to 3.0±0.5 MPa with the incorporation of BG in the fibres. Further, the deposition of hydroxycarbonate apatite on CS/PEO/BG NFs incubated in SBF was higher as compared to CS/PEO NFs. There was no difference in viability of human MSCs cultured on CS/PEO and CS/PEO/BG NFs. However, ALP activity of the MSCs on CS/PEO/BG NFs was higher than those on CS/PEO NFs. 3D stacked images of the MSCs acquired by confocal microscopy showed cell penetration in CS/PEO/BG scaffolds to the depth of 80 µm. Kandelousi et al. prepared CS/PCL NFs loaded with up to 1 wt% BG by electrospinning using a flow rate of 1 mL/h, applied voltage of 19 kV, and needle-collector distance of 16 cm [80]. The diameter of CS/PCL NFs increased from 725±322 nm for no BG to 934 nm and 814 nm for 0.5 wt% and 1 wt% BG loading, respectively. The addition of BG slightly increased hydrophilicity of the CS/PCL NFs as the water contact angle decreased slightly from 130° to 122° with BG addition. The viability and growth of human gingival fibroblasts (hGFCs) improved with the addition of 0.5 wt% BG to CS/PCL scaffolds. Lin and collaborators produced PLA NFs coated with 0.2-0.8 wt% CS by electrospinning at a flow rate of 0.5 mL/h, voltage of 21 kV, and needle-collector distance of 18 cm, respectively [81]. The produced NFs were then incubated in SBF for HAP deposition on the CS coated NFs. The average diameter of the fibres increased from 365 nm to 387 nm after CS coating and HAP deposition. In addition, the water contact angle for PLA NFs decreased from 121º to 60º with CS coating and hydrophilicity of the NFs with 0.8 wt% CS was higher than other PLA/CS NF groups. The viability, adhesion and proliferation of MG-63 osteosarcoma cells cultured on HAP-deposited, CS-coated PLA NFs was higher than the native PLA NFs, which demonstrated the importance of CS and HAP in mineralization and osteogenesis. Liverani et al. investigated the effect of BG particle size (micro or mBG versus nano or nBG) on the properties of CS/PCL NFs loaded with 30 wt% mBG/nBG. The NFs were prepared by electrospinning using a feed rate of 0.3 mL/h, voltage of 20 kV, and with needle-collector distance of 12.5 cm [82]. The average fiber diameter was found to increase with BG incorporation from 54 nm for CS/PCL fibres to 74 nm for CS/PCL/nBG and 95 nm for CS/PCL/mBG, respectively. A decrease in Young's modulus, tensile strain and tensile strength was measured for the NF composites from 3±1 MPa, 31±5 MPa, and 37±15MPa, respectively, for CSPCL NFs to 0.7±0.3 MPa, 28±4 MPa, and 17±11MPa for CS/PCL/mBG NFs and 0.27±0.04 MPa, 45±12 MPa, and 7±2 MPa for CS/PCL/nBG NFs. This decrease in mechanical properties was attributed to agglomeration of BG particles in the composites. However, there was higher HAP deposition on CS/PCL/BG NFs incubated in SBF. Thein and collaborators investigated cellular properties of HAP-deposited CS NFs. The NFs were produced by electrospinning at a voltage of 17 kV and needle-collector distance of 12 cm and then incubated in SBF for HAP deposition [83]. The average fibre diameter was 200 nm and the CaP ratio of the deposited HAP was 1.75±0.01 which was close to the mineral component of the natural bone. The rat UMR-106 osteosarcoma cells cultured on HAP-deposited CS NFs showed higher cell viability of rat UMR-106 and ALP activity as compared to those seeded on CS NFs, indicating the applicability of CS/HAP NFs in bone regeneration. Shen et al. produced CS/PVA NFs loaded with up to 1 wt% HAP by electrospinning using a flow rate of 0.5mL/h, applied voltage of 25 kV, and needle-collector distance of 10 cm [16]. The conductivity and viscosity of the electrospinning solution increased with the addition of HAP, which led to a reduction in fibre diameter. The average diameter of CS/PVA NFs decreased from 59 nm to 46 nm with the addition of 1 wt% HAP. No substantial difference in mineral deposition (Ca/P ratio) was observed on CS/PVA NFs with 0.5 wt% and 1wt% HAP content with CaP values of 1.57 and 1.56, respectively. Peng and collaborators produced HAP-enriched CS (CS/HAP) nanofibrous scaffolds at a feed rate of 2-4 mL/h, applied voltage of 20-24 kV, and needle-collector distance of 10-12 cm [84]. The cell morphology, growth, ALP expression and mRNA analysis of differentiation markers were studied using C3H10T1/2 murine MSCs. The CS/HAP NFs showed high cell adhesion and spreading during 3 days of culture owing to bioactivity of HAP. Cell spreading was evident uniformly on the entire CS/HAP NF surface whereas cell spreading was spotty on the CS NFs. Further, the rate of cell growth on CS/HAP NFs was 2-fold higher than CS NFs without HAP. mRNA expression of bone specific markers COL-I, Runx-2, ALP, and OCN were 2-fold, 2-fold 3-fold, and 3-fold higher, respectively, for the MSCs cultured on CS/HAP NFs as compared to the MSCs cultured on CS NFs. ALP activity of the MSCs cultured on CS/HAP NFs was 10% higher than those on CS NFs. The deposition of collagen by the MSCs on CS/HAP NFs was 2µg/scaffold as compared to 1.5µg/scaffold for CS NFs. Foroughi et al. prepared PHB NFs with varied ratios of CS (0-20 wt%) and nBG (0-15 wt%) using a feed rate of 1µL/h, applied voltage of 16 kV, and needle-collector distance of 16 cm [85]. The average diameters of PHB, PHB/CS with 20 wt% CS and PHB/CS/nBG with 15 wt% nBG were 8578 nm, 354 nm, and 563 nm, respectively, and the fibre diameter decreased with increasing nBG content. The addition of nBG increased hydrophilicity of the fibres as the water contact angle decreased from 58° to 44°. The best concentrations of CS and nBG with respect to mechanical strength of the NF matrices were 15 wt% and 10 wt%, respectively, and higher concentrations led to very high solution viscosities, aggregation of nBGs, and a decrease in mechanical properties. The Young's modulus, stress and strain at break for PHB/CS/nBG NFs with 15 wt% CS and 10 wt% nBG was 174-210 MPa, 2.5-3.4 MPa, and 6.5-9.0%, respectively. Enhanced mineral (calcium and phosphate) deposition with incubation in SBF for 4 weeks and decreased degradation rate over 8 weeks was observed for NFs with 15 wt% CS and 10 wt% nBG. Experimental results of Chitosan and its composite fibers using ceramics was explored widely using animal studies and the key points of few those experiments were mentioned in **Table 3.** Yang et al. produced composite NFs of CS/PV/HAP and CS with carboxyethyl chitosan and HAP (CS/CECS/HAP) by electrospinning using a feed rate, voltage and needle-collector distance of 5mL/h, 25 kV, and 8 cm, respectively [86]. The produced NFs were crosslinked with glutaraldehyde to maintain the integrity and stability of the fibre mesh. The diameter of the NFs was in the range of 100-700 nm. Mouse L929 fibroblasts cultured on CECS/PVA /HAP NF scaffolds showed higher viability as compared to CECS /PVA scaffolds.

Ghorbani et al. synthesized CS/PCL NFs doped with nano-zinc and enriched with nHAP (CS/PCL/nSn/nHAP) by electrospinning using a feed rate of 0.5-1 ml/h, voltage of 15-30 kV, and needle-collector distance of 12.5 cm [87]. The average fibre diameter increased from 136 nm for CS/PCL to 210 nm for CS/PCL//nZn/nHA composite NFs. The addition of nZn/nHAP to CS/PCL NFs increased hydrophilicity by 20-35%, as measured by water contact angle measurements. The elastic modulus and tensile strength of CS/PCL/nZn/nHAP NFs were 3-fold and 1.5-fold higher than those of CS/PCL NFs. Human adipose derived stem cells (hAD-MSCs) cultured on PCL/CS/nZn/nHAP NF scaffolds showed higher cell viability and proliferation as compared to CS/PCL scaffolds.

Table 3 : composites of chitosan with ceramics

S.N	Scaffold material	Implantation Site	Cell source	Outcome	Ref
1	CS/HAP/Genipin	Mouse calvarial bone	Mouse mesenchymal stem cells (mMSCs)	*In-vivo* biocompatibility test compared Genipin crosslinked CS/HAP and CS NFs, Micro-CT imaging showed fibres with and without HAP healed the bone defect to 35 and 10%, respectively, H&E staining showed increased cellular infiltration, ECM deposition (Masson's Trichrome staining) and integration of fiber with outer surface of the bone in crosslinked CS/HAP scaffolds as compared to crosslinked CS scaffolds, demonstrating osseointegration ability of CS/HAP NFs for bone tissue remodelling.	98
2	SF/CS/Nano HAP	Mouse subcutaneous implantation	hMSCs	Assessed ectopic bone formation using cell loaded and acellular SF/CS/Nano-HAp scaffolds, H&E and Masson's Trichrome staining showed increased cell number, tissue ingrowth and osteoid formation at the defect site using cell seeded scaffolds as compared to those without cell, Immunohistochemistry analysis showed elevated expression levels of COL-I and OCN in scaffolds with hMSCs as compared to acellular scaffolds demonstrating the potential of cellular SF/CS/nnao-HAP scaffolds for bone tissue regeneration.	99
3	Nano HAP/CS	Rat cranium	Bone marrow mesenchymal stem cells (BMSCs)	One defect implanted with nanoHAP/CS NFs seeded with BMSCs whereas contralateral defect implanted with nanoHAP/CS without cells, The entire defect site covered with new bone in scaffolds seeded with cells 20 weeks post-implantation whereas very thin bone confining only to the edges found in NFs without cells by H&E staining, Density of new bone formed at the defect site was calculated using X-ray images and the scaffolds with cells showed a significant increase in optical density, Immunohistochemical analysis showed higher expression level of osteogenic specific markers namely OCN in defect site with cells when compared to that without cells.	100
4	CS/SF/nano HAP	Subcutaneous implantation in nude mice	hMSCs	hMSCs loaded in CS/SF NFs with 30% HAP showed improved in vivo response as compared to NFs with 10% HAP and without hMSCs, CS/SF NFs with 30% nHAp scaffolds maintained excellent integrity until 2 months post-implantation and established connection with surrounding vasculature, The formation of new bone was validated by the expression of COL-I and OCN in both scaffolds, The scaffolds with cells hMSCs showed tissue mineral density (attenuation coefficient-Hounsfield Unit) of 2501 and 2351 HU/mm^2 , respectively, 2- months post-implantation, Masons trichrome assay revealed increased osteoid formation in NF scaffolds with hMSCs as compared to the scaffolds without hMSCs.	42

2. CONCLUSIONS & FUTURE CHALLENGES

The scaffold in engineered tissues provides pore volume and surface for delivery, attachment, spreading, proliferation, differentiation, and maturation of cells to the desired phenotype. Chitosan, a natural polysaccharide found in crustacean shells, is considered an ideal scaffold for regeneration of skeletal tissues like bone. It resembles the collagenous matrix of the bone tissue. It is hydrophilic, biocompatible, biodegradable, and process able to different shapes. It is amenable to chemical modification to improve its biological properties to accelerate growth of bone cells,

mineralization, and ossification. It can be blended with gelatin and alginate biopolymers to increase its hydrophilicity. It can be cross linked with glutaraldehyde or genipin to form hydrogels with predefined degradation rates. Chitosan can be formed into nano fibrous meshes by electro spinning that mimic the extracellular matrix of natural tissue with high porosity for cell loading and high surface area for cell attachment. Composite nanofiber scaffolds can be produced by blending chitosan with ceramics such as TCP, wollastonite, hydroxyapatite, or bio glass to improve mechanical strength, osteoconductivity, and bone regeneration. Future work on chemical modification of chitosan is expected to extend the application of this natural biomaterial in tissue engineering and regenerative medicine applications.

.

3. AUTHOR CONTRIBUTION STATEMENT

Dr. Nadeem Siddiqui has shared the concept and improvised the manuscript. Mr. Kotikalapudi Karthik and Miss. Monica Adapala has prepared the draft which was edited by Miss. Vemparala Renuka. Mr. Goudu Yashwanth helped in compiling the reference work and Dr. Siva Reddy Goalamri has taken care of collecting appropriate images.

,

4. CONFLICT OF INTEREST

Conflict of interest declared none

5. REFERENCES

1. Raouf GA, Gashlan H, Khedr A, Al-Jabbri H. in Vitro New Biopolymer for Bone Grafting and Bone Cement. *Int J Latest Res Sci* Technol. 2015;4(2):46-55.
2. Taichman RS. Blood and bone: two tissues whose fates are intertwined to create the hematopoietic stem-cell niche. Blood. 2005;105(7):2631-9. doi: 10.1182/blood-2004-06-2480, PMID 15585658.
3. Feng X, McDonald JM. Disorders of bone remodeling. Annu Rev Pathol. 2011;6:121-45. doi: 10.1146/annurev-pathol-011110-130203, PMID 20936937.
4. Oryan A, Monazzah S, Bigham-Sadegh A. Bone injury and fracture healing biology. Biomed Environ Sci. 2015;28(1):57-71. doi: 10.3967/bes2015.006, PMID 25566863.
5. Croisier F, Jérôme C. Chitosan-based biomaterials for tissue engineering. Eur Polym J. 2013;49(4):780-92. doi: 10.1016/j.eurpolymj.2012.12.009.
6. Rating S. Bone regeneration and repair: biology and clinical applications. Ann R Coll Surg Engl. 2006;88(3):334-. doi: 10.1308/003588406X106333c.
7. Murphy CM, O'Brien FJ, Little DG, Schindeler A. Cell-scaffold interactions in the bone tissue engineering triad. Eur Cell Mater. 2013;26:120-32. doi: 10.22203/eCM.v026a09, PMID 24052425.
8. Yuan TT, Jenkins PM, Digeorge Foushee AM, Jockheck-Clark AR, Stahl JM. Electrospun chitosan/polyethylene oxide nanofibrous scaffolds with potential antibacterial wound dressing applications. J Nanomater. 2016;2016:1-10. doi: 10.1155/2016/6231040.
9. Ho MH, Wang DM, Hsieh HJ, Liu HC, Hsien TY, Lai JY, Hou LT. Preparation and characterization of RGD-immobilized chitosan scaffolds. Biomaterials. 2005;26(16):3197-206. doi: 10.1016/j.biomaterials.2004.08.032, PMID 15603814.
10. Eltom A, Zhong G, Muhammad A. Scaffold techniques and designs in tissue engineering functions and purposes: a review. Adv Mater Sci Eng. 2019;2019:1-13. doi: 10.1155/2019/3429527.
11. Udomluck N, Koh WG, Lim DJ, Park H. Recent developments in nanofiber fabrication and modification for bone tissue engineering. Int J Mol Sci. 2019;21(1). doi: 10.3390/ijms21010099, PMID 31877799.
12. Christy PN, Basha SK, Kumari VS, Bashir AKH, Maaza M, Kaviyarasu K, Arasu MV, Al-Dhabi NA, Ignacimuthu S. Biopolymeric nanocomposite scaffolds for bone tissue engineering applications – a review. J Drug Deliv Sci Technol. 2020;55. doi: 10.1016/j.jddst.2019.101452, PMID 101452.
13. Sill TJ, von Recum HA. Electrospinning: applications in drug delivery and tissue engineering. Biomaterials. 2008;29(13):1989-2006. doi: 10.1016/j.biomaterials.2008.01.011, PMID 18281090.
14. Chahal S, Kumar A, Hussian FSJ. Development of biomimetic electrospun polymeric biomaterials for bone tissue engineering. A review. J Biomater Sci Polym Ed. 2019;30(14):1308-55. doi: 10.1080/09205063.2019.1630699, PMID 31181982.
15. Haider S, Al-Zeghayer Y, Ahmed Ali FA, Haider A, Mahmood A, Al-Masry WA, Imran M, Aijaz MO. Highly aligned narrow diameter chitosan electrospun nanofibers. J Polym Res. 2013;20(4). doi: 10.1007/s10965-013-0105-9.
16. Kai S. Preparation of chitosan bicomponent nanofibers filled with hydroxyapatite nanoparticles via electrospinning. J Appl Polym Sci. 2009;115(4):2683-90. doi: 10.1002/app.29832.
17. Thie A. Encyclopedia of nanotechnology; 2012. doi: 10.1007/978-90-481-9751-4.
18. Fourie J, Taute F, du Preez L, de Beer D. Chitosan composite biomaterials for bone tissue engineering—a review. Regen Eng Transl Med Published online 2020, doi: 10.1007/s40883-020-00187-7.
19. Younes I, Rinaudo M. Chitin and chitosan preparation from marine sources. Structure, properties and applications. Mar Drugs. 2015;13(3):1133-74. doi: 10.3390/md13031133, PMID 25738328.
20. Sultankulov B, Berillo D, Sultankulova K, Tokay T, Saparov A. Progress in the development of chitosan-based biomaterials for tissue engineering and regenerative medicine. Biomolecules. 2019;9(9). doi: 10.3390/biom9090470, PMID 31509976.
21. Siddiqui N, Pramanik K. Effects of micro and Nano β-TCP fillers in freeze-gelled chitosan scaffolds for bone tissue engineering. J Appl Polym Sci. 2014;131(21):1-10. doi: 10.1002/app.41025.
22. Dass CR, Choong PF. The use of chitosan formulations in cancer therapy. J Microencapsul. 2008;25(4):275-9. doi: 10.1080/02652040801970461, PMID 18465306.
23. Ojeda-Hernández DD, Canales-Aguirre AA, Matias-Guiu J, Gomez-Pinedo U, Mateos-Díaz JC. Potential of

chitosan and its derivatives for biomedical applications in the central nervous system. Front Bioeng Biotechnol. 2020;8:389. doi: 10.3389/fbioe.2020.00389, PMID 32432095.
24. Chiang MT, Yao HT, Chen HC. Effect of dietary chitosans with different viscosity on plasma lipids and lipid peroxidation in rats fed on a diet enriched with cholesterol. Biosci Biotechnol Biochem. 2000;64(5):965-71. doi: 10.1271/bbb.64.965, PMID 10879465.
25. Park PJ, Je JY, Kim SK. Free radical scavenging activity of chitooligosaccharides by electron spin resonance spectrometry. J Agric Food Chem. 2003;51(16):4624-7. doi: 10.1021/jf034039+, PMID 14705887.
26. Kumari A, Yadav SK, Yadav SC. Biodegradable polymeric nanoparticles based drug delivery systems. Colloids Surf B Biointerfaces. 2010;75(1):1-18. doi: 10.1016/j.colsurfb.2009.09.001, PMID 19782542.
27. Qi L, Xu Z. In vivo antitumor activity of chitosan nanoparticles. Bioorg Med Chem Lett. 2006;16(16):4243-5. doi: 10.1016/j.bmcl.2006.05.078, PMID 16759859.
28. Siddiqui N, Pramanik K, Jabbari E. Osteogenic differentiation of human mesenchymal stem cells in freeze-gelled chitosan/Nano β-tricalcium phosphate porous scaffolds crosslinked with genipin. Mater Sci Eng C Mater Biol Appl. 2015;54:76-83. doi: 10.1016/j.msec.2015.05.005, PMID 26046270.
29. Hoseinpour Najar MH, Minaiyan M, Taheri A. Preparation and in vivo evaluation of a novel gel-based wound dressing using arginine–alginate surface-modified chitosan nanofibers. J Biomater Appl. 2018;32(6):689-701. doi: 10.1177/0885328217739562, PMID 29119880.
30. Siddiqui N, Madala S, Rao Parcha S, Mallick SP. Osteogenic differentiation ability of human mesenchymal stem cells on chitosan/poly (caprolactone)/Nano beta tricalcium phosphate composite scaffolds. Biomed Phys Eng Express. 2020;6(1):015018. doi: 10.1088/2057-1976/ab6550, PMID 33438606.
31. Mallick SP, Beyene Z, Suman DK, Madhual A, Singh BN, Srivastava P. Strategies towards orthopaedic tissue engineered graft generation: current scenario and application. Biotechnol Bioprocess Eng. 2019;24(6):854-69. doi: 10.1007/s12257-019-0086-6.
32. Islam MM, Shahruzzaman M, Biswas S, Nurus Sakib M, Rashid TU. Chitosan based bioactive materials in tissue engineering applications-A review. Bioact Mater. 2020;5(1):164-83. doi: 10.1016/j.bioactmat.2020.01.012, PMID 32083230.
33. Du F, Wang H, Zhao W, Li D, Kong D, Yang J, Zhang Y. Gradient nanofibrous chitosan/poly e{open}-caprolactone scaffolds as extracellular microenvironments for vascular tissue engineering. Biomaterials. 2012;33(3):762-70. doi: 10.1016/j.biomaterials.2011.10.037, PMID 22056285.
34. Ozcelik B, Brown KD, Blencowe A, Daniell M, Stevens GW, Qiao GG. Ultrathin chitosan-poly(ethylene glycol) hydrogel films for corneal tissue engineering. Acta Biomater. 2013;9(5):6594-605. doi: 10.1016/j.actbio.2013.01.020, PMID 23376126.
35. Tao F, Cheng Y, Shi X, Zheng H, Du Y, Xiang W, Deng H. Applications of chitin and chitosan nanofibers in bone regenerative engineering. Carbohydr Polym. 2020;230:115658. doi: 10.1016/j.carbpol.2019.115658.
36. Meng ZX, Zheng W, Li L, Zheng YF. Fabrication, characterization and in vitro drug release behavior of electrospun PLGA/chitosan nanofibrous scaffold. Mater Chem Phys. 2011;125(3):606-11. doi: 10.1016/j.matchemphys.2010.10.010.
37. Zhou Z, Yan D, Cheng X, Kong M, Liu Y, Feng C, Chen X. Biomaterials based on N,N,N-trimethyl chitosan fibers in wound dressing applications. Int J Biol Macromol. 2016;89:471-6. doi: 10.1016/j.ijbiomac.2016.02.036, PMID 26893050.
38. Siddiqui N, Pramanik K. Development of fibrin conjugated chitosan/Nano b -TCP composite scaffolds with improved cell supportive property for bone tissue Regeneration. 2015;41534:1-10. doi: 10.1002/app.41534.
39. Adithya SP, Sidharthan DS, Abhinandan R, Balagangadharan K, Selvamurugan N. Nanosheets-incorporated bio-composites containing natural and synthetic polymers/ceramics for bone tissue engineering. Int J Biol Macromol. 2020;164:1960-72. doi: 10.1016/j.ijbiomac.2020.08.053, PMID 32800960.
40. Howk D, Chu TMG. Design variables for mechanical properties of bone tissue scaffolds. *Tech Pap ISA*. Biomed Sci Instrum. 2006;42(Cdc):278-83. PMID 16817621.
41. Aidun A, Safaei Firoozabady A, Moharrami M, Ahmadi A, Haghighipour N, Bonakdar S, Faghihi S. Graphene oxide incorporated polycaprolactone/chitosan/collagen electrospun scaffold: enhanced osteogenic properties for bone tissue engineering. Artif Organs. 2019;43(10):E264-81. doi: 10.1111/aor.13474, PMID 31013365.
42. Lai GJ, Shalumon KT, Chen JP. Response of human mesenchymal stem cells to intrafibrillar nanohydroxyapatite content and extrafibrillar nanohydroxyapatite in biomimetic chitosan/silk fibroin/nanohydroxyapatite nanofibrous membrane scaffolds. Int J Nanomedicine. 2015;10:567-84. doi: 10.2147/IJN.S73780, PMID 25609962.
43. Chen P, Liu L, Pan J, Mei J, Li C, Zheng Y. Biomimetic composite scaffold of hydroxyapatite/gelatin-chitosan core-shell nanofibers for bone tissue engineering. Mater Sci Eng C Mater Biol Appl. 2019;97:325-35. doi: 10.1016/j.msec.2018.12.027, PMID 30678918.
44. Ghorbani M, Nezhad-Mokhtari P, Sohrabi H, Roshangar L. Electrospun chitosan/nanocrystalline cellulose-graft-poly(N-vinylcaprolactam) nanofibers as the reinforced scaffold for tissue engineering. J Mater Sci. 2020;55(5):2176-85. doi: 10.1007/s10853-019-04115-1.
45. Ezati M, Safavipour H, Houshmand B, Faghihi S. Development of a PCL/gelatin/chitosan/β-TCP electrospun composite for guided bone regeneration. Prog Biomater. 2018;7(3):225-37. doi: 10.1007/s40204-018-0098-x, PMID 30242739.
46. Jalaja K, Naskar D, Kundu SC, James NR. Potential of electrospun core-shell structured gelatin-chitosan nanofibers for biomedical applications. Carbohydr Polym. 2016;136:1098-107. doi: 10.1016/j.carbpol.2015.10.014, PMID 26572452.
47. Ma X, Wu G, Dai F, et al. Chitosan/polydopamine layer by layer self-assembled silk fibroin nanofibers for biomedical applications. Carbohydr Polym.

2021;251(June 2020):117058. doi: 10.1016/j.carbpol.2020.117058.
48. Mak YW, Leung WWF. Crosslinking of genipin and autoclaving in chitosan-based nanofibrous scaffolds: structural and physicochemical properties. J Mater Sci. 2019;54(15):10941-62. doi: 10.1007/s10853-019-03649-8.
49. Toskas G, Cherif C, Hund RD, Laourine E, Mahltig B, Fahmi A, Heinemann C, Hanke T. Chitosan(PEO)/silica hybrid nanofibers as a potential biomaterial for bone regeneration. Carbohydr Polym. 2013;94(2):713-22. doi: 10.1016/j.carbpol.2013.01.068, PMID 23544625.
50. Tsai RY, Kuo TY, Hung SC, Lin CM, Hsien TY, Wang DM, Hsieh HJ. Use of gum arabic to improve the fabrication of chitosan-gelatin-based nanofibers for tissue engineering. Carbohydr Polym. 2015;115:525-32. doi: 10.1016/j.carbpol.2014.08.108, PMID 25439928.
51. Zhao X, Chen S, Lin Z, Du C. Reactive electrospinning of composite nanofibers of carboxymethyl chitosan cross-linked by alginate dialdehyde with the aid of polyethylene oxide. Carbohydr Polym. 2016;148:98-106. doi: 10.1016/j.carbpol.2016.04.051, PMID 27185120.
52. Zarei M, Samimi A, Khorram M, Abdi MM, Golestaneh SI. Fabrication and characterization of conductive polypyrrole/chitosan/collagen electrospun nanofiber scaffold for tissue engineering application. Int J Biol Macromol. 2021;168:175-86. doi: 10.1016/j.ijbiomac.2020.12.031, PMID 33309657.
53. Esbah Tabaei PS, Asadian M, Ghobeira R, Cools P, Thukkaram M, Derakhshandeh PG, Abednatanzi S, Van Der Voort P, Verbeken K, Vercruysse C, Declercq H, Morent R, De Geyter N. Combinatorial effects of coral addition and plasma treatment on the properties of chitosan/polyethylene oxide nanofibers intended for bone tissue engineering. Carbohydr Polym. 2021;253(September):117211. doi: 10.1016/j.carbpol.2020.117211.
54. Balagangadharan K, Trivedi R, Vairamani M, Selvamurugan N. Sinapic acid-loaded chitosan nanoparticles in polycaprolactone electrospun fibers for bone regeneration in vitro and in vivo. Carbohydr Polym. 2019;216:1-16. doi: 10.1016/j.carbpol.2019.04.002, PMID 31047045.
55. Estrada-Villegas GM, Del Río-De Vicente JI, Argueta-Figueroa L, González-Pérez G. UV-initiated crosslinking of electrospun chitosan/poly(ethylene oxide) nanofibers doped with ZnO-nanoparticles: development of antibacterial nanofibrous hydrogel. MRS Commun. 2020;10(4):642-51. doi: 10.1557/mrc.2020.74, PMID 33398240.
56. Hadipour-Goudarzi E, Montazer M, Latifi M, Aghaji AAG. Electrospinning of chitosan/sericin/PVA Nanofibers Incorporated within *situ* synthesis of Nano silver. Carbohydr Polym. 2014;113:231-9. doi: 10.1016/j.carbpol.2014.06.082, PMID 25256480.
57. Jin S, Li J, Wang J, Jiang J, Zuo Y, Li Y, Yang F. Electrospun silver ion-loaded calcium phosphate/chitosan antibacterial composite fibrous membranes for guided bone regeneration. Int J Nanomedicine. 2018;13:4591-605. doi: 10.2147/IJN.S167793, PMID 30127608.
58. Sambudi NS, Kim MG, Bin PS. The formation of a web-like connection among electrospun chitosan/PVA fiber networks by the reinforcement of ellipsoidal calcium carbonate. Mater Sci Eng C. 2016;60:518-25. doi: 10.1016/j.msec.2015.11.079.
59. Satpathy A, Pal A, Sengupta S, Das A, Hasan MM, Ratha I, Barui A, Bodhak S. Bioactive nano-hydroxyapatite doped electrospun PVA-chitosan composite nanofibers for bone tissue engineering applications. J Indian Inst Sci. 2019;99(3):289-302. doi: 10.1007/s41745-019-00118-8.
60. Toloue EB, Karbasi S, Salehi H, Rafienia M. Potential of an electrospun composite scaffold of poly (3-hydroxybutyrate)-chitosan/alumina nanowires in bone tissue engineering applications. Mater Sci Eng C Mater Biol Appl. 2019;99(December 2018):1075-91. doi: 10.1016/j.msec.2019.02.062, PMID 30889640.
61. Talebian S, Mehrali M, Mohan S, Balaji raghavendran Hr, Mehrali M, Khanlou HM, Kamarul T, Afifi AM, Abass AA. Chitosan (PEO)/bioactive glass hybrid nanofibers for bone tissue engineering. RSC Adv. 2014;4(90):49144-52. doi: 10.1039/C4RA06761D.
62. Saatchi A, Arani AR, Moghanian A, Mozafari M. Synthesis and characterization of electrospun cerium-doped bioactive glass/chitosan/polyethylene oxide composite scaffolds for tissue engineering applications. Ceram Int. 2021;47(1):260-71. doi: 10.1016/j.ceramint.2020.08.130.
63. Govindasamy K, Dahlan NA, Janarthanan P, Goh KL, Chai SP, Pasbakhsh P. Electrospun chitosan/polyethylene-oxide (PEO)/halloysites (HAL) membranes for bone regeneration applications. Appl Clay Sci. 2020;190. doi: 10.1016/j.clay.2020.105601, PMID 105601.
64. Arab-Ahmadi S, Irani S, Bakhshi H, Atyabi F, Ghalandari B. Immobilization of carboxymethyl chitosan/laponite on polycaprolactone nanofibers as osteoinductive bone scaffolds. Polym Adv Technol. 2021;32(2):755-65. doi: 10.1002/pat.5128.
65. Fadaie M, Mirzaei E, Geramizadeh B, Asvar Z. Incorporation of nanofibrillated chitosan into electrospun PCL nanofibers makes scaffolds with enhanced mechanical and biological properties. Carbohydr Polym. 2018;199:628-40. doi: 10.1016/j.carbpol.2018.07.061, PMID 30143171.
66. Yang S, Lei P, Shan Y, Zhang D. Preparation and characterization of antibacterial electrospun chitosan/poly (vinyl alcohol)/graphene oxide composite nanofibrous membrane. Appl Surf Sci. 2018;435:832-40. doi: 10.1016/j.apsusc.2017.11.191.
67. Topsakal A, Uzun M, Ugar G, Ozcan A, Altun E, Oktar FN, Ikram F, Ozkan O, Turkoglu Sasmazel H, Gunduz O. Development of amoxicillin-loaded electrospun polyurethane/chitosan/β-tricalcium phosphate scaffold for bone tissue regeneration. IEEE Trans Nanobiosci. 2018;17(3):321-8. doi: 10.1109/TNB.2018.2844870, PMID 29994218.
68. Sharifi F, Atyabi SM, Norouzian D, Zandi M, Irani S, Bakhshi H. Polycaprolactone/carboxymethyl chitosan nanofibrous scaffolds for bone tissue engineering application. Int J Biol Macromol. 2018;115:243-8. doi: 10.1016/j.ijbiomac.2018.04.045, PMID 29654862.
69. Su CJ, Tu MG, Wei LJ, Hsu TT, Kao CT, Chen TH, Huang TH. Calcium silicate/chitosan-coated electrospun poly (lactic acid) fibers for bone tissue

engineering. Materials (Basel). 2017;10(5). doi: 10.3390/ma10050501, PMID 28772861.
70. Song J, Remmers SJA, Shao J, Kolwijck E, Walboomers XF, Jansen JA, Leeuwenburgh SC, Yang F. Antibacterial effects of electrospun chitosan/poly(ethylene oxide) nanofibrous membranes loaded with chlorhexidine and silver. Nanomedicine. 2016;12(5):1357-64. doi: 10.1016/j.nano.2016.02.005, PMID 26970025.
71. Januariyasa IK, Ana ID, Yusuf Y. Nanofibrous poly(vinyl alcohol)/chitosan contained carbonated hydroxyapatite nanoparticles scaffold for bone tissue engineering. Mater Sci Eng C Mater Biol Appl. 2020;107:110347. doi: 10.1016/j.msec.2019.110347.
72. Hokmabad VR, Davaran S, Aghazadeh M, Alizadeh E, Salehi R, Ramazani A. A comparison of the effects of silica and hydroxyapatite nanoparticles on poly(ε-caprolactone)-poly(ethylene glycol)-poly(ε-caprolactone)/chitosan nanofibrous scaffolds for bone tissue engineering. Tissue Eng Regen Med. 2018;15(6):735-50. doi: 10.1007/s13770-018-0140-z, PMID 30603592.
73. Frohbergh ME, Katsman A, Botta GP, Lazarovici P, Schauer CL, Wegst UG, Lelkes PI. Electrospun hydroxyapatite-containing chitosan nanofibers crosslinked with genipin for bone tissue engineering. Biomaterials. 2012;33(36):9167-78. doi: 10.1016/j.biomaterials.2012.09.009, PMID 23022346.
74. Zhang Y, Venugopal JR, El-Turki A, Ramakrishna S, Su B, Lim CT. Electrospun biomimetic nanocomposite nanofibers of hydroxyapatite/chitosan for bone tissue engineering. Biomaterials. 2008;29(32):4314-22. doi: 10.1016/j.biomaterials.2008.07.038, PMID 18715637.
75. Zhang S, Prabhakaran MP, Qin X, Ramakrishna S. Biocomposite scaffolds for bone regeneration: role of chitosan and hydroxyapatite within poly-3-hydroxybutyrate-co-3-hydroxyvalerate on mechanical properties and in vitro evaluation. J Mech Behav Biomed Mater. 2015;51:88-98. doi: 10.1016/j.jmbbm.2015.06.032, PMID 26232670.
76. Zhang Y, Reddy VJ, Wong SY, Li X, Su B, Ramakrishna S, Lim CT. Enhanced biomineralization in osteoblasts on a novel electrospun biocomposite nanofibrous substrate of hydroxyapatite/collagen/chitosan. Tissue Eng Part A. 2010;16(6):1949-60. doi: 10.1089/ten.TEA.2009.0221, PMID 20088700.
77. Zhao X, Zhou L, Li Q, Zou Q, Du C. Biomimetic mineralization of carboxymethyl chitosan nanofibers with improved osteogenic activity in vitro and in vivo. Carbohydr Polym. 2018;195(March):225-34. doi: 10.1016/j.carbpol.2018.04.090, PMID 29804972.
78. Shalumon KT, Sowmya S, Sathish D, Chennazhi KP, Nair SV, Jayakumar R. Effect of incorporation of nanoscale bioactive glass and hydroxyapatite in PCL/chitosan nanofibers for bone and periodontal tissue engineering. J Biomed Nanotechnol. 2013;9(3):430-40. doi: 10.1166/jbn.2013.1559, PMID 23620999.
79. Pangon A, Saesoo S, Saengkrit N, Ruktanonchai U, Intasanta V. Hydroxyapatite-hybridized chitosan/chitin whisker bionanocomposite fibers for bone tissue engineering applications. Carbohydr Polym. 2016;144:419-27. doi: 10.1016/j.carbpol.2016.02.053, PMID 27083834.
80. Kandelousi PS, Rabiee SM, Jahanshahi M, Nasiri F. The effect of bioactive glass nanoparticles on polycaprolactone/chitosan scaffold: melting enthalpy and cell viability. J Bioact Compat Polym. 2019;34(1):97-111. doi: 10.1177/0883911518819109.
81. Lin CC, Fu SJ, Lin YC, Yang IK, Gu Y. Chitosan-coated electrospun PLA fibers for rapid mineralization of calcium phosphate. Int J Biol Macromol. 2014;68:39-47. doi: 10.1016/j.ijbiomac.2014.04.039, PMID 24768970.
82. Liverani L, Lacina J, Roether JA, Boccardi E, Killian MS, Schmuki P, Schubert DW, Boccaccini AR. Incorporation of bioactive glass nanoparticles in electrospun PCL/chitosan fibers by using benign solvents. Bioact Mater. 2018;3(1):55-63. doi: 10.1016/j.bioactmat.2017.05.003, PMID 29744442.
83. Van Hong Thien D, Hsiao SW, Ho MH, Li CH, Shih JL. Electrospun chitosan/hydroxyapatite nanofibers for bone tissue engineering. J Mater Sci. 2013;48(4):1640-5. doi: 10.1007/s10853-012-6921-1.
84. Peng H, Yin Z, Liu H, Chen X, Feng B, Yuan H, Su B, Ouyang H, Zhang Y. Electrospun biomimetic scaffold of hydroxyapatite/chitosan supports enhanced osteogenic differentiation of mMSCs. Nanotechnology. 2012;23(48):485102. doi: 10.1088/0957-4484/23/48/485102, PMID 23128604.
85. Foroughi MR, Karbasi S, Khoroushi M, Khademi AA. Polyhydroxybutyrate/chitosan/bioglass nanocomposite as a novel electrospun scaffold: fabrication and characterization. J Porous Mater. 2017;24(6):1447-60. doi: 10.1007/s10934-017-0385-2.
86. Yang D, Jin Y, Zhou Y, Ma G, Chen X, Lu F, Nie J. In situ mineralization of hydroxyapatite on electrospun chitosan-based nanofibrous scaffolds. Macromol Biosci. 2008;8(3):239-46. doi: 10.1002/mabi.200700221, PMID 18322911.
87. Ghorbani FM, Kaffashi B, Shokrollahi P, Seyedjafari E, Ardeshirylajimi A. PCL/chitosan/Zn-doped nHA electrospun nanocomposite scaffold promotes adipose derived stem cells adhesion and proliferation. Carbohydr Polym. 2015;118:133-42. doi: 10.1016/j.carbpol.2014.10.071, PMID 25542118.
88. Lotfi G, Shokrgozar MA, Mofid R, Abbas FM, Ghanavati F, Baghban AA, Yavari SK, Pajoumshariati S. Biological evaluation (in vitro and in vivo) of bilayered collagenous coated (Nano electrospun and solid wall) chitosan membrane for periodontal guided bone regeneration. Ann Biomed Eng. 2016;44(7):2132-44. doi: 10.1007/s10439-015-1516-z, PMID 26586588.
89. Ho MH, Yao CJ, Liao MH, Lin PI, Liu SH, Chen RM. Chitosan nanofiber scaffold improves bone healing via stimulating trabecular bone production due to upregulation of the Runx2/osteocalcin/alkaline phosphatase signaling pathway. Int J Nanomedicine. 2015;10:5941-54. doi: 10.2147/IJN.S90669, PMID 26451104.
90. Kang YM, Lee BN, Ko JH, Kim GH, Kang KN, Kim DY, Kim JH, Park YH, Chun HJ, Kim CH, Kim MS. In vivo biocompatibility study of electrospun chitosan microfiber for tissue engineering. Int J Mol Sci. 2010;11(10):4140-8. doi: 10.3390/ijms11104140, PMID 21152326.
91. Su H, Liu KY, Karydis A, et al. In vitro and in vivo evaluations of a novel post-electrospinning treatment to improve the fibrous structure of chitosan membranes for guided bone regeneration. Biomed

Mater. 2017;12(1):15003. doi: 10.1088/1748-605X/12/1/015003.
92. Gniesmer S, Brehm R, Hoffmann A, de Cassan D, Menzel H, Hoheisel AL, Glasmacher B, Willbold E, Reifenrath J, Ludwig N, Zimmerer R, Tavassol F, Gellrich NC, Kampmann A. Vascularization and biocompatibility of poly(ε-caprolactone) fiber mats for rotator cuff tear repair. PLOS ONE. 2020;15(1):e0227563. doi: 10.1371/journal.pone.0227563, PMID 31929570.
93. Datta P, Ghosh P, Ghosh K, Maity P, Samanta SK, Ghosh SK, Mohapatra PK, Chatterjee J, Dhara S. In vitro ALP and osteocalcin gene expression analysis and in vivo biocompatibility of n-methylene phosphonic chitosan nanofibers for bone regeneration. J Biomed Nanotechnol. 2013;9(5):870-9. doi: 10.1166/jbn.2013.1592, PMID 23802418.
94. Zhao J, Han W, Chen H, Tu M, Huan S, Miao G, Zeng R, Wu H, Cha Z, Zhou C. Fabrication and in vivo osteogenesis of biomimetic poly(propylene carbonate) scaffold with nanofibrous chitosan network in macropores for bone tissue engineering. J Mater Sci Mater Med. 2012;23(2):517-25. doi: 10.1007/s10856-011-4468-3, PMID 22042464.
95. Costa-Pinto AR, Martins AM, Castelhano-Carlos MJ, Correlo VM, Sol PC, Longatto-Filho A, Battacharya M, Reis RL, Neves NM. In vitro degradation and in vivo biocompatibility of chitosan-poly(butylene succinate) fiber mesh scaffolds. J Bioact Compat Polym. 2014;29(2):137-51. doi: 10.1177/0883911514521919.
96. Jung UW, Song KY, Kim CS, Lee YK, Cho KS, Kim CK, Choi SH. Effects of a chitosan membrane coated with polylactic and polyglycolic acid on bone regeneration in a rat calvarial defect. Biomed Mater. 2007;2(3):S101-5. doi: 10.1088/1748-6041/2/3/S03, PMID 18458451.
97. Gomes SR, Rodrigues G, Martins GG, Roberto MA, Mafra M, Henriques CM, Silva JC. In vitro and in vivo evaluation of electrospun nanofibers of PCL, chitosan and gelatin: A comparative study. Mater Sci Eng C Mater Biol Appl. 2015;46:348-58. doi: 10.1016/j.msec.2014.10.051, PMID 25491997.
98. Frohbergh M, Katsmann A, Mondrinos M, Stabler C, Hankenson K, Oristaglio J, Lelkes P, Isales CM, Hill WD. Stromal cell-derived factor-1β potentiates bone morphogenetic protein-2-stimulated osteoinduction of genetically engineered bone marrow-derived mesenchymal stem cells in vitro. Tissue Eng Part A. Published online. 2013;19(1-2):1-13. doi: 10.1089/ten.TEA.2012.0085, PMID 22779446.
99. Shalumon KT, Lai GJ, Chen CH, Chen JP. Modulation of bone-specific tissue regeneration by incorporating bone morphogenetic protein and controlling the shell thickness of silk fibroin/chitosan/nanohydroxyapatite core-shell nanofibrous membranes. ACS Appl Mater Interfaces. 2015;7(38):21170-81. doi: 10.1021/acsami.5b04962, PMID 26355766.
100. Liu H, Peng H, Wu Y, Zhang C, Cai Y, Xu G, Li Q, Chen X, Ji J, Zhang Y, OuYang HW. The promotion of bone regeneration by nanofibrous hydroxyapatite/chitosan scaffolds by effects on integrin-BMP/Smad signaling pathway in BMSCs. Biomaterials. 2013;34(18):4404-17. doi: 10.1016/j.biomaterials.2013.02.048, PMID 23515177.